Journal for ImmunoTherapy of Cancer

Stromal cells modulate innate immune cell phenotype and function in colorectal cancer via the Sialic acid/Siglec axis

Aoise O'Neill [1,2,3] Norashikin Zakaria [1,3] Courtney Bull,[4] Hannah Egan,[1,2,3] Shania M Corry,[4,5] Niamh A Leonard,[1,2,3] Clodagh O'Meara [1,2,3] Linda Howard [2] Anastasija Walsh,[1,3] Eileen Reidy,[1,2,3,6] Jenny Che [7] Li Peng,[7] Lizhi Cao [7] Laurence J Egan,[1,3] Thomas Ritter [2,6] Margaret Sheehan,[8] Aoife Canney,[8] Kevin Culligan,[8] Aisling M Hogan,[3,9] Sean O Hynes,[8,10] Philip D Dunne,[4,11] Michael O'Dwyer,[3,12] Oliver Treacy [1,2,3] Aideen E Ryan [1,2,3,6]

To cite: O'Neill A, Zakaria N, Bull C, *et al*. Stromal cells modulate innate immune cell phenotype and function in colorectal cancer via the Sialic acid/Siglec axis. *Journal for ImmunoTherapy of Cancer* 2025;**13**:e012491. doi:10.1136/jitc-2025-012491

► Additional supplemental material is published online only. To view, please visit the journal online (https://doi.org/10.1136/jitc-2025-012491).

OT and AER contributed equally.

Accepted 15 September 2025

For numbered affiliations see end of article.

Correspondence to
Professor Aideen E Ryan; aideen.ryan@universityofgalway.ie

ABSTRACT

Background The immunosuppressive tumor microenvironment reduces immune response effectiveness in stromal-rich tumors, including consensus molecular subtype 4 colorectal cancer (CRC). Mesenchymal stromal cells (MSCs), precursors to cancer-associated fibroblasts (CAFs), promote cancer progression by suppressing anti-tumor immune responses. Hypersialylation of glycans on tumors engages Siglec receptors on immune cells, driving immune dysfunction, but its role in stromal-mediated suppression of innate immunity remains unclear.

Methods Sialylation, Sialic acids and Siglec ligands were measured on CRC tissue, primary human normal-associated fibroblasts (NAFs), CAFs, and tumor-conditioned MSCs (MSC^{TCS}) using transcriptional profiles, immunohistochemistry and flow cytometry, respectively. The effect of stromal cell sialylation on macrophages and NK cells was assessed in *ex vivo* human primary stromal and immune cell co-cultures, and expression of Siglec-10 and immune cell phenotype markers and function was measured by flow cytometry and real-time imaging. Using an immunocompetent Balb/c CT26 mouse model, we induced tumors with/without conditioned stromal cells, with/without pretreatment of stromal cells with sialyltransferase inhibitor (3FAX) or sialidase (E610). We assessed the effect of stromal cell sialylation on macrophages and NK cells in the tumor and secondary lymphoid tissues by flow cytometry.

Results Stromal cells, including CAFs, in CRC tumors are highly sialylated compared with epithelial cancer cells and are associated with high expression of the sialyltransferase *ST6GALNAC6*. Genetic knockdown of *ST6GALNAC6* reduced the expression of stromal cell Siglec-10 ligands in MSCs. CAFs and MSC^{TCS} induced Siglec-10 on macrophages and NK cells and impaired macrophage phagocytosis and NK cell cytotoxicity. Sialidase treatment reduced Siglec-10 expression, restoring macrophage and NK cell antitumor functions. *In vivo* and *ex vivo*, desialylation of stromal cells increased macrophage activation ($CD11b^{+}CD80^{+}$) and reduced immunosuppressive marker expression (CD206, PD-L1, Siglec-G) in lymphoid tissues, indicating sustained systemic anti-tumor immunity. Intratumoral NK cells exhibited high Siglec-G expression and impaired cytotoxicity, and granzyme B expression significantly increased with sialidase treatment of stromal cells. In an inflammatory tumor model, inflammatory tumor-conditioned MSCs (MSC^{iTCS}) promoted metastasis and Siglec-G induction on NK cells and macrophages, both reversed by sialyltransferase inhibition, underscoring the effects of stromal modulation of innate immune cell function in inflammatory tumors.

Conclusions Stromal cell sialylation modulates innate immune suppression in CRC via the sialic acid/Siglec axis. Targeting stromal sialylation restores NK cytotoxicity and macrophage activation, offering novel insights that may shape therapeutic strategies for reversing immunosuppression in stromal-rich tumors.

WHAT IS ALREADY KNOWN ON THIS TOPIC

⇒ The tumor microenvironment (TME) of consensus molecular subtype 4 colorectal cancer (CRC) is associated with high stromal burden, poor immune infiltration, resistance to anti-cancer therapies and thus poor patient prognosis. Immune checkpoint inhibitors (ICIs) have limited impact on stromal-rich CRC tumors, therefore, highlighting the need to discover and target novel mechanisms of tumor immune evasion.

⇒ Emerging studies have highlighted that stromal cells in CRC and pancreatic ductal adenocarcinoma (PDAC) are highly sialylated, expressing even higher levels of sialic acid on their cell surface than epithelial cancer cells. Targeting stromal cell sialylation has yielded promising data in restoring the anti-tumor activity of T cells and macrophages. There is a clear need to explore the effects of targeting stromal cell sialylation on other immune cells of the TME and to evaluate the Siglec/sialic acid axis of stromal and immune cells in ICI-resistant CRC tumors.

WHAT THIS STUDY ADDS

⇒ We identify that *ST6GALNAC6*, a sialyltransferase enzyme, regulates the production of Siglec-10 ligands in CRC stromal cells. Overexpression of *ST6GALNAC6* and Siglec-10 correlated with poor survival in CRC and mesenchymal CRC tumors.

⇒ We show for the first time an induction of Siglec-10 expression on macrophages and NK cells in stromal-immune co-culture experimental models with hypersialylated MSCs and CAFs *in vitro* and *ex vivo*. Targeting sialylation increased macrophage phagocytosis and NK cell cytotoxicity of CRC cells, indicating a direct functional role for stromal cell sialylation in immunosuppression.

⇒ An immunogenic mouse model of CRC was used to evaluate the potential therapeutic efficacy of targeting stromal cell sialylation in overcoming stromal cell-mediated immunosuppression in CRC. Sialic acid-targeting of stroma slowed tumor growth and reduced inflammation-driven metastasis. This was associated with greater infiltration and activation of macrophages and NK cells, highlighting stromal cell sialylation as a mechanism of innate immune cell suppression in stromal-rich CRC.

HOW THIS STUDY MIGHT AFFECT RESEARCH, PRACTICE OR POLICY

⇒ Our research provides insight into a novel mechanism of stromal cell-mediated immunosuppression of innate immune cells in CRC and may open up new avenues of research for targeting stromal cells in stromal-rich TMEs such as pancreatic, breast, and ovarian cancers.

⇒ Our research identifies a stromal cell effect of enhancing Siglec expression on tumor-infiltrating innate immune cells as a novel immune checkpoint, which may be useful in identifying potential novel immunotherapeutic combinations in the future.

INTRODUCTION

Colorectal cancer (CRC) is the second-leading cause of cancer mortality worldwide, primarily due to late-stage diagnosis and resistance to current therapies.[1] Advances in immunotherapies for CRC have been largely unsuccessful, except for microsatellite instable (MSI) tumors, which represent only 15% of all CRC. In microsatellite stable (MSS) tumors, immunosuppression within the tumor microenvironment (TME) is a major therapeutic challenge.[2] CRC can be classified into four consensus molecular subtypes (CMS) based on transcriptional and mutational profiles.[3] CMS1 is associated with high immune cell infiltration, BRAF mutations, and good response to therapy, largely due to its enrichment in MSI tumors.[4] Conversely, mesenchymal subtype CMS4 CRC, which has high stromal burden and poor prognosis, is enriched with MSS tumors.[5] Enrichment for MSS tumors and the presence of stromal cells and inflammatory signatures are associated with the worst disease-free survival rates in CMS4 CRC.[6] Therefore, novel therapeutic approaches are urgently needed.

The CMS4 TME is highly complex and heterogeneous, comprising cancer cells, stromal cells, immune cells, extracellular matrix, and secreted factors. Stromal cells of mesenchymal origin, which include mesenchymal stromal cells (MSCs) and cancer-associated fibroblasts (CAF), predominate the CRC TME and expansion of these cells promotes tumor growth, angiogenesis, metastasis, and drug resistance.[7] There is growing evidence that their ability to potently induce immunosuppression is a predominant and targetable mechanism of tumor promotion,[8–14] and the immunomodulatory properties of stromal cells have been well established.[15 16] CMS4 tumors are also dominated by tumor-associated macrophages (TAMs) with a pro-tumor phenotype.[17] Although stromal cells are a desirable target for immunotherapy, their inherent heterogeneity makes targeting difficult, as MSCs and CAFs have limited specific markers and share many similarities with normal fibroblasts.[18] Therefore, identifying predominant mechanisms of action in tumor promotion, such as those that induce immunosuppression, is of significant interest and may hold promise to reinvigorate anti-tumor immunity and improve outcomes in CRC.

The cancer-immunity cycle now includes the impact of stromal cells in shaping the immunosuppressive landscape in the TME, including the CRC TME.[19] $CD8^+$ cytotoxic T cells have been shown to reside in the stroma of CRC, preventing them from infiltrating and killing tumor cells.[20] Macrophages in CRC have been shown to be polarized to an anti-inflammatory, pro-tumorigenic phenotype.[17] Natural killer (NK) cells have reduced cytotoxicity of cancer cells in the presence of stromal cells.[9] The mechanisms of stromal-immune modulation have been of significant interest in recent years.[21–23] Recent evidence from our group and others suggests that post-translational sialylation may be important in regulating stromal cell immunoregulatory functions.[20 24]

Sialylation, a post-translational process involving sialic acid addition to glycoproteins and glycolipids, plays a vital role in cellular communication and immune modulation.[25 26] The biosynthesis and degradation of sialylated ligands is regulated by the expression of sialyltransferases (STs) and sialidases, respectively.[27] Hypersialylation has been linked to immune evasion in many cancers, including breast, lung, pancreatic, and multiple myeloma.[26] Binding of sialylated ligands to sialic-acid binding immunoglobulin-like lectins (Siglecs) can impair immune function.[26] There are 14 human Siglecs, Siglec 1–15, which are expressed differentially on innate and adaptive immune cells, and 3 mouse orthologues Siglec-E, -G, and -F.[28 29] Once bound by sialic acid, Siglecs have either a downstream immunoreceptor tyrosine-based inhibition motif (ITIM) or immunoreceptor tyrosine-based activation motif (ITAM), which inhibits or activates immune responses via SHP1/2 or SYK activation, respectively.[29] Siglec-7, -9 and -10 are the most well-characterized Siglecs and are expressed on T cells, NK cells, and macrophages.[30–32] Tumor and stromal cells in the TME can exploit this pathway to evade immune surveillance by expressing Siglec ligands.[33 34] Some Siglec ligands (Siglec-L) have also been discovered in recent years in the TME and include PSGL-1, CD43 (Siglec-7L), CD52, and CD24 (Siglec-10L).[35–38] Although Siglec interactions have been studied as novel immune checkpoints,

the mechanisms by which they are expressed and function as immunosuppressive checkpoints in the TME are not fully elucidated.[39 40]

Here, we assessed sialylation across CRC CMS subtypes and show that CRC stromal cells express high levels of sialic acid glycans and are enriched for sialylation gene signatures. STs are upregulated in CRC stroma, and targeting *ST6GALNAC6* reduced Siglec-10 ligand expression. Stromal-rich CRC is enriched for Siglec-10 and Siglec-10 ligands, and we show that Siglec-10 overexpression in the TME of high fibroblast (Hi-Fi) tumors is associated with poor survival outcome in CRC. We observed that stromal cells induced Siglec-10 expression on primary human macrophages, which was associated with reduced tumor cell phagocytosis. Induction of Siglec-10 on NK cells was reversed by targeting the sialic acid/Siglec axis and enhanced NK cell cytotoxicity. In a preclinical tumor model, stromal cells induced Siglec-10 on macrophages and pre-targeting of stromal cell sialylation reduced Siglec-G expression by macrophages, while increasing the frequency of CD80-expressing macrophages, as well as granzyme B-expressing and cytotoxic NK cells in tumors. TNF-α-mediated inflammatory conditioning of stromal cells induced Siglec-G expressing macrophages and NK cells in the TME, which were reversed by targeting the sialic acid/Siglec axis and were associated with lower levels of invasion. Together, these data highlight an integral role for the sialic acid/Siglec axis in stromal-rich CRC and demonstrate that targeting stromal cell sialic acid/Siglec interactions modulates innate immune contexture and may represent an innovative strategy to enhance antitumor immunity.

RESULTS

CRC stromal cells express high levels of sialoglycans

CMS subtype stratification reveals distinctive cellular features of the TME with prognostic implications.[41] CMS4, the mesenchymal subtype, is associated with high stromal infiltration, poor prognosis, and limited response to chemotherapy and immunotherapy.[3 41 42] We analyzed transcriptional profiles of untreated stage II/III colon cancer (CC) tumors across CMS molecular subtypes (n=258) (GSE39582) (figure 1A).[3] Single sample gene set enrichment analysis (ssGSEA) compared the enrichment of pathways related to glycosylation and sialylation (figure 1B). Glycosylation was significantly lower in CMS4 relative to the other subtypes (figure 1C, left). Sialylation-related pathways such as protein sialylation, sialic acid binding, and α2,3 ST activity were increased in CMS4 relative to the other subtypes (figure 1C). 2,6 ST activity genes were either unchanged or lower in CMS4 (online supplemental figure 1A). We assessed the surface expression of α2–6-linked and α2–3-linked sialic acid in CRC using immunohistochemistry (figure 1D). Both α2–3-linked and α2–6-linked sialic acids are expressed in CRC as indicated by MAL-II (α2–3) and SNA-I (α2–6) binding, respectively (figure 1D, left). SNA-I binding was higher than MAL-II in CRC tissue, and MAL-II was significantly higher in the stromal region compared with epithelial region (figure 1D, right), as determined using QuPath (online supplemental figure 1B). We assessed α2–3-linked and α2–6-linked sialic acid expression in the CMS4 CRC cell lines SW480, CACO2, and HCT116, and stromal cells using an *ex vivo* conditioning model with MSCs. MSCs were conditioned with HCT116 tumor cell secretome (TCS) and TNF-α-activated inflammatory TCS (iTCS), (referred to as MSC^{TCS} and MSC^{iTCS}) (figure 1E).[17] Flow cytometric analysis demonstrated that MSCs express higher levels of both α2,3 and α2,6-linked sialic acid compared with CMS4-like CRC cell lines (figure 1F). MSC^{TCS} express α2,6-linked sialic acid, which was further enhanced in MSC^{iTCS}, while α2,3-linked sialic acid expression was high and did not change with TCS or iTCS conditioning. Taken together, these data indicate that sialylation is enriched in CMS4 tumors and stromal cells are more highly sialylated.

STs are upregulated in the stroma of CRC, and targeting *ST6GALNAC6* reduces Siglec-10 ligand expression on stromal cells

Sialylation is regulated through ST and neuraminidase (NEU) activity. We therefore assessed ST and NEU gene expression using ConfoundR[34–36] (https://confoundr.qub.ac.uk/), a web application that enables visualization of gene expression in epithelial and stromal compartments across CRC datasets (GSE35602, GSE39396) (online supplemental figure 2A).[37] *ST3GAL1-6*, *ST6GALNAC3*, *ST6GALNAC5*, *ST6GALNAC6*, and *ST8SIA1* were more highly expressed in the stromal compartment compared with the epithelium in most patient samples (GSE53602, figure 2A). Neuraminidases (NEUs), which cleave sialic acids, were either unchanged between stroma and epithelium (*NEU1-3*) or decreased in the stromal compartment (*NEU4*) (figure 2A). Notably, *ST3GAL1*, *ST3GAL5*, and *ST6GALNAC6* were enriched in fibroblasts and leukocytes (dataset GSE39396; online supplemental figure 2B). We then measured ST expression in primary CRC CAFs isolated from tumor biopsies (online supplemental figure 2C). All ST3 genes, except for *ST3GAL6*, were expressed by CAFs, while the only ST6 genes expressed were *ST6GALNAC2*, *ST6GALNAC4* and *ST6GALNAC6* (figure 2B). Bulk RNA-seq data from mouse stromal cells showed that ST6GALNAC6 expression was significantly higher on conditioned MSC^{iTCS} (online supplemental figure 2D,E). Kaplan-Meier plotter analysis (https://kmplot.com/analysis/)[43] showed that high *ST6GALNAC6* expression significantly correlated with lower overall survival (OS) in CRC and in CMS4 CRC patients (figure 2C). The prognostic significance of *ST6GALNAC6* expression with relapse-free survival (RFS) in CRC was assessed in a validation cohort (GSE39582). Kaplan-Meier survival analysis revealed that patients with high *ST6GALNAC6* expression had significantly poorer RFS compared with those with low expression (log-rank p=0.00089), with an HR of 2.33 (95% CI:

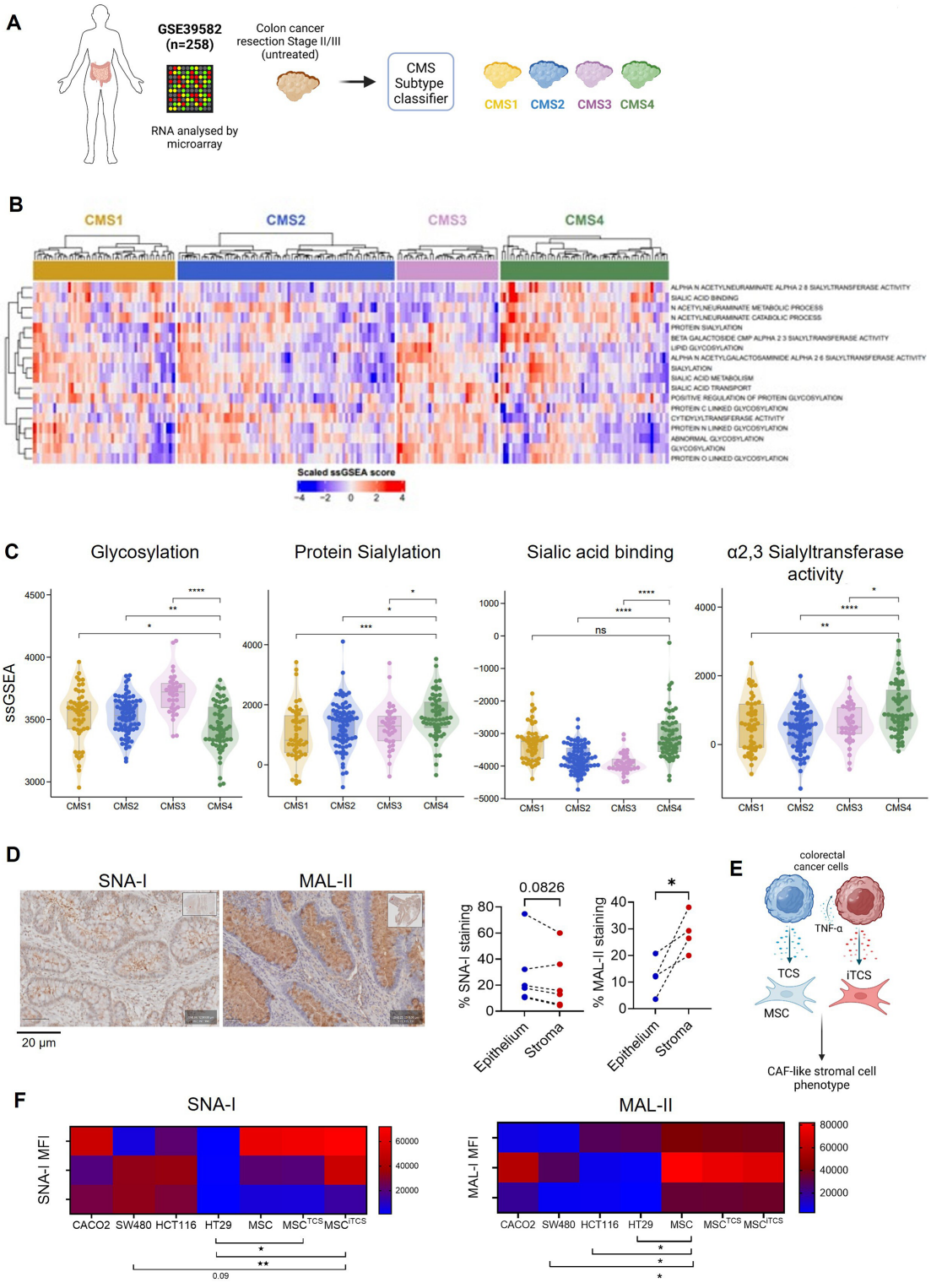

Figure 1 Sialylation is upregulated in CMS4 colorectal cancer. (A) Transcriptional profiles of stage II/III untreated colon cancer samples (GSE39582) were retrieved and CMS classified (n=258; CMS1=49, CMS2=75, CMS3=35, CMS4=58). (B) Expression heatmap of transcriptional signatures of glycosylation and sialylation-related genes across CMS1–4 subtypes. (C) Single sample gene set enrichment analysis (ssGSEA) of pathways associated with glycosylation, protein sialylation, sialic acid binding, and α2,3 sialyltransferase activity. (D) Immunohistochemical (IHC) staining images of lectins SNA-I and MAL-II in CRC tissue sections and their quantification in epithelial and stromal regions. (E) Experimental outline of MSC conditioning with tumor cell secretome (TCS) and TNF-α-treated inflammatory TCS (iTCS). (F) Heatmaps showing MFI for SNA-I and MAL-II expression in CRC cell lines, unconditioned MSC, MSC^{TCS} and MSC^{iTCS}. Data are mean±SD; *p<0.05, **p<0.01, ***p<0.001, ****p<0.0001 by Wilcoxon rank-sum test, CMS4 as the reference group (C), paired t-test (D) or one-way ANOVA followed by Tukey's post hoc test (F). ANOVA, analysis of variance; CMS4, consensus molecular subtype 4; CRC, colorectal cancer; MFI, median fluorescence intensity; MSC, mesenchymal stromal cell.

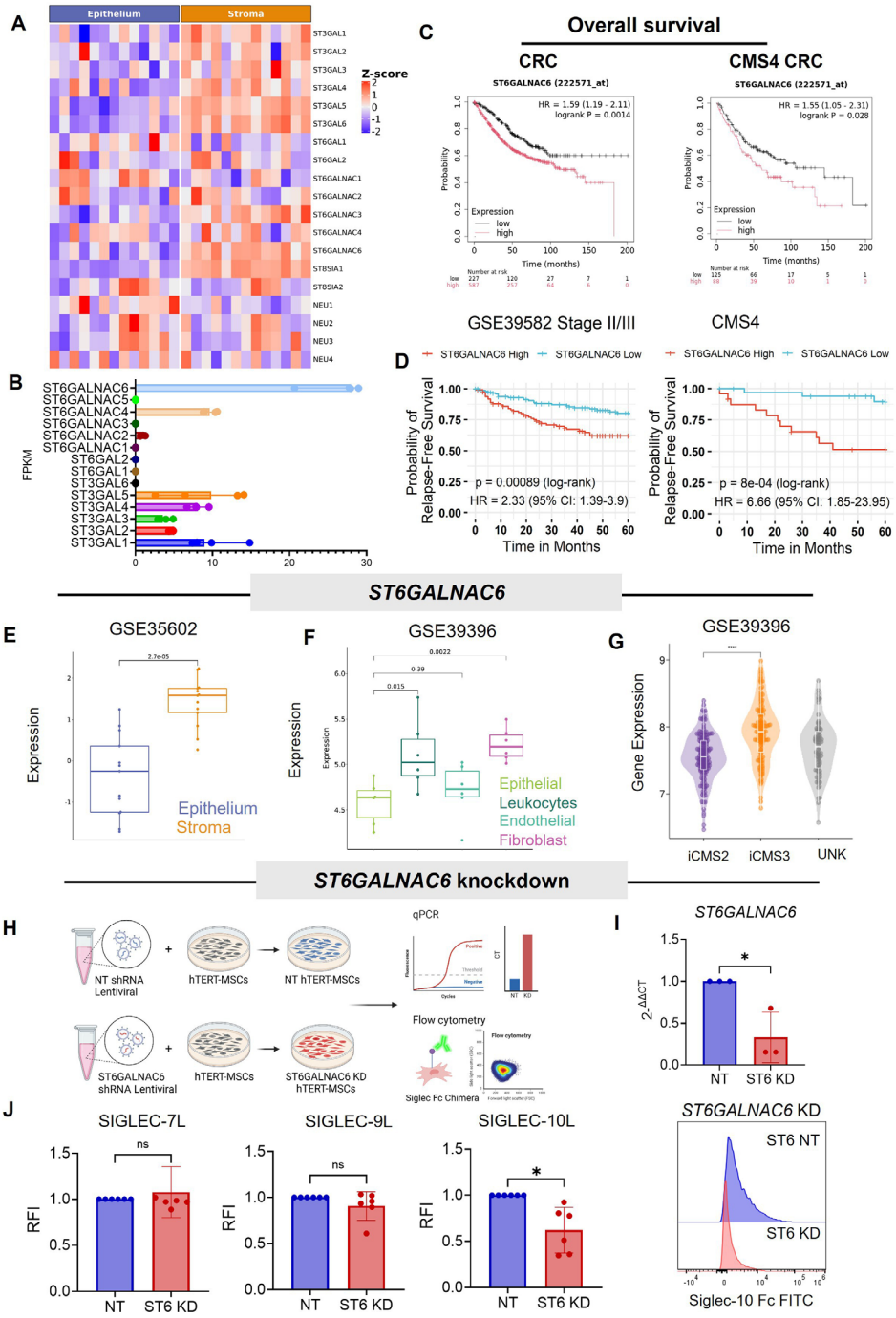

Figure 2 Sialyltransferases are upregulated in colorectal cancer, and targeting *ST6GALNAC6* reduces Siglec-10 ligand expression by stromal cells. (A) Expression heatmap of sialyltransferase and neuraminidase genes in stromal and epithelial compartments in human CRC samples (n=13) created by ConfoundR (dataset GSE35602). (B) Fragments per kilobase of exon per million mapped fragments (FPKM) values of sialyltransferase genes in human CRC-derived cancer-associated fibroblasts (CAFs) (n=4), analyzed by bulk RNA sequencing. (C) Overall survival (OS) analysis for *ST6GALNAC6* high-expression and low-expression in CRC (left) and CMS4 CRC samples (right). Kaplan-Meier survival curve showing log-rank test p value generated using KMPlotter. (D) Kaplan-Meier plot showing probability of relapse-free survival of *ST6GALNAC6* high-expression and low-expression in stage II/III untreated CRC (left) and in CMS4 CRC samples (right) (both from GSE39582 dataset). Kaplan-Meier survival curves showing log-rank test p value. (E, F) *ST6GALNAC6* gene expression in different cells of CRC samples created by ConfoundR (datasets GSE35602 and GSE39396). (G) *ST6GALNAC6* gene expression in iCMS2 and iCMS3 CRC samples (dataset GSE39396). (H) Experimental outline for *ST6GALNAC6* shRNA knockdown in hTERT-MSCs. (I) Relative expression of *ST6GALNAC6* in hTERT-MSCs after shRNA knockdown (ST6 KD) compared with non-targeting (NT) shRNA controls (n=3). (J) Relative fluorescence intensity (RFI) (normalized to NT hTERT-MSCs) of Siglec-7, Siglec-9, and Siglec-10 ligand expression in *ST6GALNAC6* KD (ST6 KD) hTERT-MSCs (n=6) and representative overlay histograms for Siglec-10 ligand expression. Data are mean±SD; *p<0.05, ****p<0.0001 using Wilcoxon rank-sum test (E–G) or paired t-test (I, J). CRC, colorectal cancer; hTERT, human telomerase reverse transcriptase; MSC, mesenchymal stromal cell.

1.39 to 3.90), indicating a strong association between high *ST6GALNAC*6 expression and poorer outcomes. In CMS4 patients, high *ST6GALNAC6* expression had significantly poorer RFS compared with those with low expression (log-rank p=0.0008), with an HR of 6.66 (95% CI: 1.85 to 23.95) (figure 2D). To evaluate whether high *ST6GALNAC6* is an independent prognostic factor, multivariable Cox proportional hazards regression was performed. After adjustment, significant predictors included high *ST6GALNAC6* (HR=2.24, 95% CI: 1.30 to 3.83, p=0.003), male sex (HR=2.12, 95% CI: 1.21 to 3.70, p=0.008) and TNM stage 3 (HR=2.89, 95% CI: 1.67 to 5.02, p<0.001). CMS subtype classification did not reach statistical significance in this model (online supplemental figure 2F). Furthermore, *ST6GALNAC6* expression was significantly higher in stroma (GSE35602 dataset, figure 2E) and fibroblasts compared with epithelial cells (GSE39396, figure 2F). *ST6GALNAC6* expression was also higher in CMS4 tumors (online supplemental figure 2G) and poor prognosis iCMS3 stromal-rich CRC tumors (figure 2G).

We next investigated the role of *ST6GALNAC6* in sialylated ligand expression. Using an immortalized stromal cell line (human telomerase reverse transcriptase (hTERT)-MSCs), we generated a stable genetic knockdown (KD) of *ST6GALNAC6* using lentiviral-mediated delivery of shRNA. We confirmed that hTERT-MSCs were highly sialylated; comparable to primary hMSCs, based on α2,3-linked and α2,6-linked sialic acid expression (online supplemental figure 3A). Non-targeting (NT) control was used to assess KD specificity (figure 2H). We confirmed significant reduction of *ST6GALNAC6* gene expression in KD MSCs (figure 2I). As Siglec-7, Siglec-9 and Siglec-10 have been shown to be immunosuppressive in cancer,[44] we measured Siglec-7 ligand (Siglec-7L), Siglec-9 ligand (Siglec-9L), and Siglec-10 ligand (Siglec-10L) expression using Siglec Fc Chimeras. Stromal cells expressed Siglec-7L, Siglec-9L and Siglec-10L (online supplemental figure 3B) at baseline, which was increased by TCS/iTCS conditioning (Siglec-7L and Siglec-10L). We assessed the effect of *ST6GALNAC6* KD on sialylated ligands and observed no significant differences in Siglec-7L and Siglec-9L expression (figure 2J, left and middle), but we observed a significant reduction in Siglec-10L expression with *ST6GALNAC6* KD compared with NT control (figure 2J, right). Taken together, these data suggest that *ST6GALNAC6* is highly expressed in CRC stromal cells, and its expression is involved in the production of Siglec-10L.

Stromal-rich CRC is enriched for Siglec-10 receptor and ligands and is associated with low RFS

Siglec receptors are expressed on various immune cells, and ligand binding triggers inhibitory signals via ITIM and SHP1/2 signaling.[45] In CRC, Siglec expression was higher in the stromal compartment than epithelium (online supplemental figure 4A). CMS-classified transcriptional profiles were analyzed by a waterfall plot (GSE39582, figure 3A) and boxplot (figure 3B). CMS4 tumors had significantly higher Siglec-10 gene expression compared with CMS2-3 tumors. CMS1 tumors expressed similar levels of Siglec-10 (figure 3B). Siglec-10 expression was significantly higher in high-fibroblast CRC tumors (GSE39582, figure 3C) and positively correlated with fibroblast activation protein (FAP) and negatively correlated with the epithelial marker, EpCAM, (cBioportal, online supplemental figure 4B). In a second cohort (GSE39582), Siglec-10 had the most significant correlation with FAP, compared with Siglec-7 and Siglec-9 receptors (figure 3D, online supplemental figure 4C). High Siglec-10 expression is predictive of a lower probability of RFS in CRC and CMS4 tumors compared with low Siglec-10 expression (figure 3E,F). Of note, very few tumors expressed low levels of Siglec-10. These observations were validated in a second cohort of CRC patients (E-MTAB 863) (online supplemental figure 4D–G).

Next, we measured the expression of Siglec-10 in CRC patient-derived peripheral blood mononuclear cells (PBMCs), specifically $CD3^+$ T cells ($CD4^+$ and $CD8^+$ T cells) and $CD3^-$ cells ($CD56^+$ NK cells and $CD14^+CD16^+$ monocytes) (gating strategy, online supplemental figure 5A,B). Siglec-10 was highly expressed on $CD56^+$ NK cells and $CD14^+/CD14^+CD16^+$ monocyte/macrophage subsets (figure 3G). Siglec-10L was increased on MSC^{TCS} and MSC^{iTCS} (online supplemental figure 3B) and was significantly higher on MSC^{iTCS} compared to either HCT116 (figure 3H, left) or SW480 (figure 3H, right) CRC cells.

The ST inhibitor 3FaxNeu5Ac (3FAX) inhibits stromal cell sialylation effectively over a period of 6 days in culture.[20] CAFs expressed higher Siglec-10L compared with HCT116, and the expression was significantly reduced with 3FAX treatment, confirming sialylation-dependent binding (figure 3I). CD24 and CD52, two known ligands for Siglec-10, were also expressed on MSC^{iTCS} (figure 3K), with CD52 also being highly expressed in CMS4 CRC tumors of the FOCUS cohort (online supplemental figure 5C). To assess Siglec-10 localization in CRC tumors, we performed multiplex immunofluorescence staining for Siglec-10 and CD24, which showed Siglec-10 expression was predominantly localized within the stromal compartment of CRC tissue, while CD24 was predominantly in epithelial regions (figure 3J, online supplemental figure 5D). These data show Siglec-10 receptor and ligand-expressing cells are enriched in the stromal compartment of CRC.

Stromal cells induce Siglec-10 expression on primary human macrophages and NK cells and inhibit cytotoxicity which can be targeted via the sialic acid/Siglec axis

Macrophages are one of the most abundant immune cells in the TME of CRC. In CMS4 CRC, macrophages exhibit reduced anti-tumor function.[17] We observed high Siglec-10 expression on macrophages and NK cells and therefore asked whether the sialic acid/Siglec axis is involved in macrophage-mediated immunosuppression. We observed strong positive correlations between Siglec-10, CD14, and

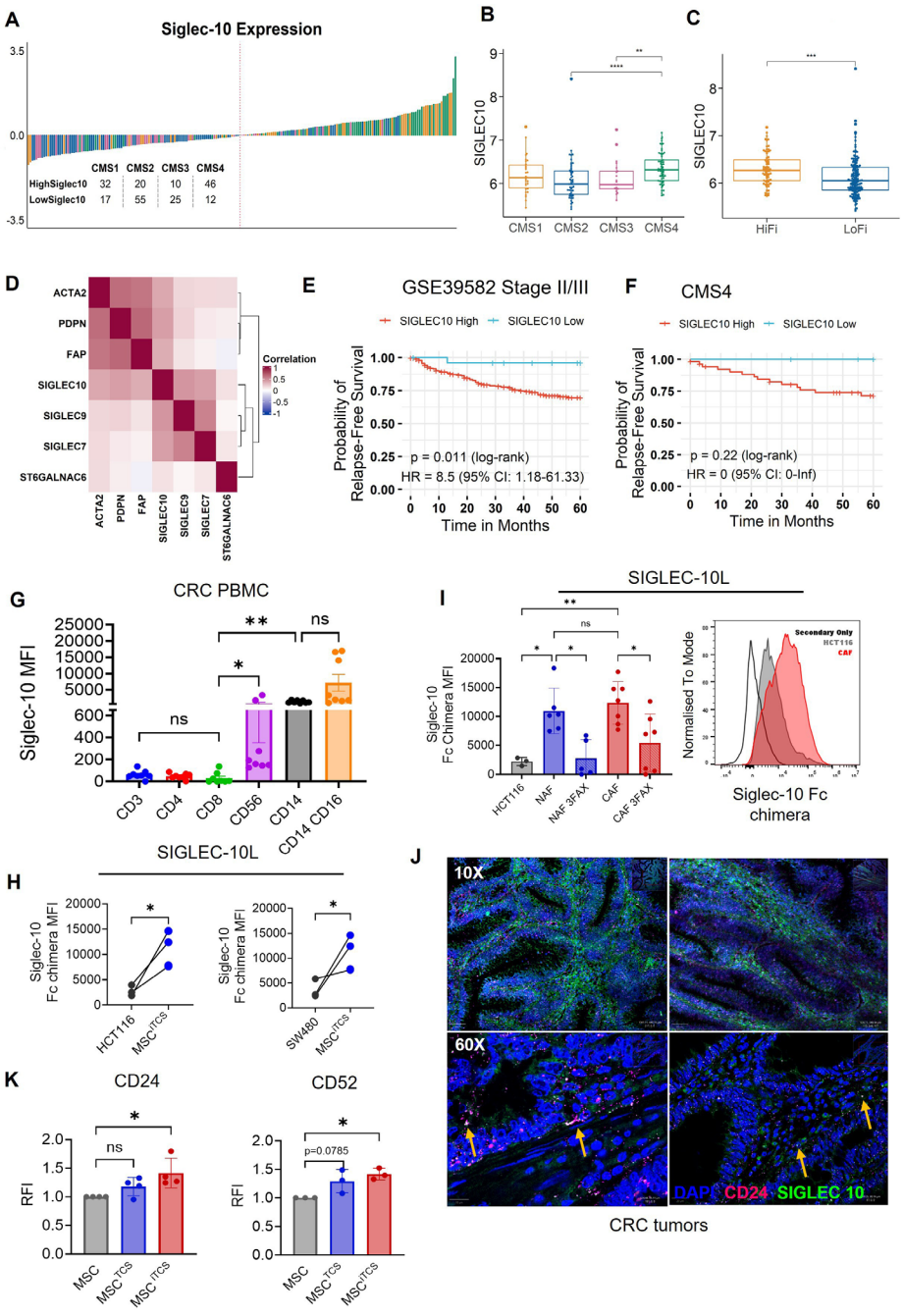

Figure 3 Stromal-rich colorectal cancer enriched for Siglec-10 and Siglec-10 ligand and associated with poor prognosis. (A) Waterfall plot depicting high and low Siglec-10 expression across CMS subtypes (dataset GSE39582). (B, C) Siglec-10 expression levels across CMS subtypes, in high fibroblast (HiFi) and low fibroblast (LoFi) CRC samples (dataset GSE39582). (D) Heatmap showing correlation between stromal cell genes (ACTA2, PDPN, FAP), Siglec-7, Siglec-9 and Siglec-10 receptor, and *ST6GALNAC6* gene. (E, F) Kaplan-Meier plots showing probability of relapse-free survival of Siglec-10 high-expression and low-expression in stage II/III untreated CRC and in CMS4 CRC samples (both from GSE39582 dataset). Kaplan-Meier survival curves showing log-rank test p value. (G) Median fluorescence intensity (MFI) of Siglec-10 expression by immune cell subsets in peripheral blood mononuclear cells (PBMCs) from CRC samples (n=8). (H) MFI of Siglec-10 Fc chimera (Siglec-10 ligand) expression by HCT116 and SW480 CRC cells and MSC^{iTCS} (n=3). (I) MFI of Siglec-10 Fc chimera (Siglec-10 ligand) expression by CAFs and normal-associated fibroblasts (NAFs) ± 3FAX pre-treatment (n=5–7) and overlay histograms showing representative CAF and HCT116 expression. (J) Confocal microscopy images of multiplex immunofluorescence staining of CD24 (pink) and Siglec-10 (green) in CRC tissue sections (DAPI nuclear staining shown in blue). (K) Relative fluorescence intensity (RFI: relative to MSCs) of CD24 and CD52 expression by MSC, MSC^{TCS} and MSC^{iTCS}. Data are mean±SD; *p<0.05, **p<0.01, ***p<0.001, ****p<0.0001 by Wilcoxon rank-sum test (B, C), non-parametric Kruskal-Wallis test (G), unpaired Welch's t test (H) and ordinary one-way ANOVA followed by Tukey's post hoc test (I, K). ANOVA, analysis of variance; CAF, cancer-associated fibroblast; CMS, consensus molecular subtype; CRC, colorectal cancer; RFI, relative fluorescence intensity; TCS, tumor cell secretome.

CD16 mRNA expression (cBioportal, CRC TCGA, online supplemental figure 6A). To understand if the TME impacts expression of Siglec-10 on macrophages, we used an indirect co-culture of primary human macrophages ± IFN-γ and IL-4 (pro-inflammatory), or IL-4 alone (anti-inflammatory) with tumor secretome (TCS or iTCS) or MSC^{TCS} or MSC^{iTCS} secretome (figure 4A). We observed no increase of Siglec-10 on naïve, pro-inflammatory, or anti-inflammatory macrophages with HCT116 TCS or iTCS (figure 4B, online supplemental figure 6B,C). In contrast, Siglec-10 expression was significantly increased on naïve, pro-inflammatory, and anti-inflammatory macrophage in co-culture with MSC^{iTCS} (figure 4C), indicating a stromal-specific increase of Siglec-10 following co-culture with inflammatory CRC stroma. To confirm these effects in primary human NAFs and CAFs, we set up a direct co-culture with primary macrophages isolated from PBMCs and measured Siglec-10 expression on $CD11b^+$ macrophages (figure 4D). To assess whether this was sialic acid-dependent, NAFs and CAFs were treated with two different sialic acid-targeting molecules and strategies, ST inhibitor P-3Fax-Neu5Ac (3FAX) (stromal cell pre-treatment) and E610 bi-sialidase (E610) (Palleon Pharmaceutical) (stromal cell pre-treatment and PBMC co-culture). Both molecules target sialic acid via different mechanisms (figure 4D, bottom). Both 3FAX and E610 effectively reduce SNA-I, MAL-II, and stromal cell Siglec ligand expression. We also assessed PNA-1 as a measure of de-sialylation and confirmed increased binding to similar levels using both strategies (online supplemental figure 6D–F). We observed a significant increase in Siglec-10 expression by $CD11b^+$ macrophages when co-cultured with CAFs, but not with NAFs (figure 4E). Treatment of stromal cell co-cultures with E610 significantly reduced Siglec-10 expression by $CD11b^+$ macrophages (figure 4E, left), but this was not observed with 3FAX pre-treatment of CAFs and NAFs (figure 4E, right). To assess the impact of tumor or stromal cells on macrophage anti-tumor effector functions, we used an Incucyte cell imaging phagocytosis assay. We observed a suppression of phagocytosis following co-culture with iTCS stromal-conditioned pro-inflammatory macrophages when compared with tumor-conditioned (figure 4F,G and online supplemental figure 6G). Collectively, these data show that stromal cells selectively induce Siglec-10 receptor expression on primary human macrophages in a sialic acid-dependent manner, which can be reversed by targeting the sialic acid/Siglec axis with E610. This enhanced Siglec-10 expression is associated with suppression of tumor cell phagocytosis.

NK cells play an essential role in anti-tumor immunity. They recognize and kill tumor cells without prior sensitization, although NK cell function is often impaired in solid tumors[46] and is suppressed by interactions with stromal cells.[47] NK cells express high levels of Siglec receptors which affect their cytotoxic functions.[48] Siglec-10 was expressed at high levels on $CD56^+$ NK cells from CRC PBMCs (figure 5A). cBioportal analysis showed a positive correlation of Siglec-10 with CD56 mRNA expression in CRC (figure 5B). We co-cultured NAFs and CAFs with stimulated PBMCs (figure 5C) or sorted and expanded human NK cells (figure 5F) and measured Siglec-10 expression on $CD56^+$ NK cells (figure 5D). We observed a significant increase in the frequency of Siglec-10 expressing $CD56^+$ NK cells following co-culture with CAFs, which was not affected by pre-treatment of stromal cells with 3FAX, as shown by both frequency and MFI of Siglec-10 on $CD56^+$ NK cells (figure 5Ei). However, with E610 treatment of stromal and immune cells, we observed a significant reduction in Siglec-10-expressing $CD56^+$ NK cells, indicating a sialic acid-dependent mechanism (figure 5Eii). Next, we assessed the effects of stromal cells on NK cells isolated and expanded from PBMCs (figure 5F). NK cells were expanded, characterized and co-cultured with NAFs and CAFs. We observed a significant increase in frequency and MFI of Siglec-10 on $CD56^+$ NK cells following co-culture with CAFs compared with NAFs (figure 5G). NK cells were recovered from stromal co-cultures and subsequently co-cultured with HCT116 cells to assess NK cytotoxicity (figure 5H). NK cytotoxicity was unaffected by 3FAX-targeting of NAFs or CAFs (figure 5H, left two graphs). However, NK cytotoxicity was significantly induced by E610 pre-treated CAFs (figure 5H, right). These data show for the first time that CAFs induce Siglec-10 expression on NK cells and pre-treatment of stroma with sialidase increases NK cell anti-tumor effector cytotoxicity.

Macrophages *in vivo* are suppressed by CRC stroma, which is reversed systemically with sialic acid targeting of stromal cells

It has been well established that macrophages have prognostic implications in many tumors, including CRC.[49] Using an immunocompetent Balb/c subcutaneous tumor model, we assessed the effects of pre-targeting stromal cell sialylation on innate immune cell phenotypes in tumors, draining lymph nodes (DLN), and spleens at day 21 (figure 6A). To do this, we induced CT26 tumors in the presence or absence of MSC^{TCS} including pre-treatment of MSC^{TCS} with 3FAX or E610. MSC^{TCS} promoted CT26 tumor growth over time, as previously observed,[50] and stromal cell desialylation led to significantly reduced tumor growth at day 16 (figure 6B). The effect on tumor growth was not fully sustained until day 21, although a significant increase was not seen in $MSC^{TCS\,E610}$ at 21 days (figure 6B).

We assessed the tumor-associated phenotype of macrophages, specifically CD206, PD-L1, and Siglec-G expression on $CD45^+CD11b^+$ macrophages in the tumor, DLN, and spleen by flow cytometry. Macrophages expressing CD206 and PD-L1 are associated with tumor progression, metastasis, and immune suppression in CRC.[51 52] We observed significantly higher frequencies of $CD206^+$– (figure 6C, Left), $PD\text{-}L1^+$– (figure 6C, middle) and $Siglec\text{-}G^+$-expressing (figure 6C, right) $CD11b^+$ macrophages in the tumor compared with the secondary lymphoid tissues, indicating that the TME selectively induces a

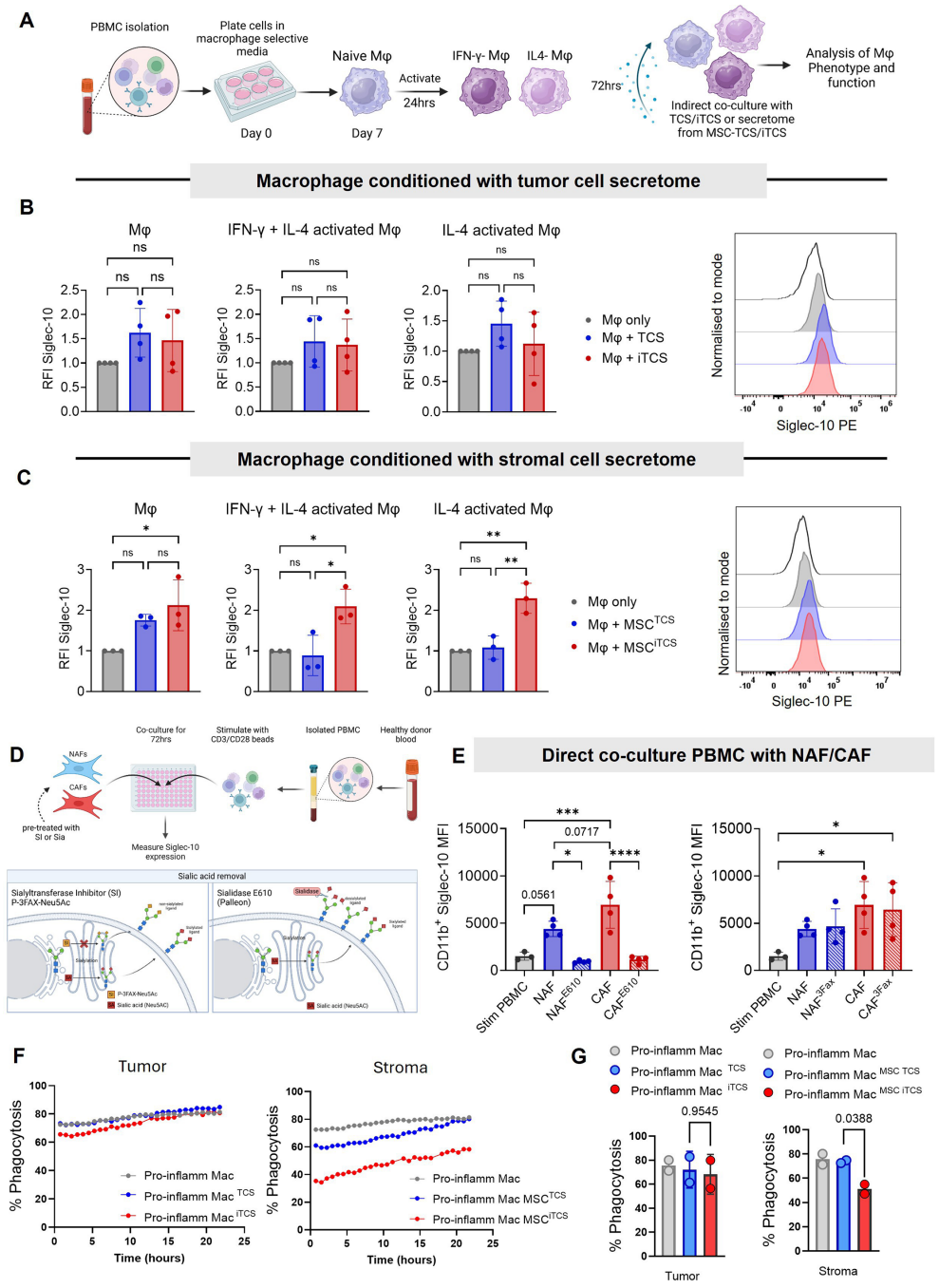

Figure 4 Stromal cells induce Siglec-10 expression on primary human macrophages and are associated with suppressed tumor cell phagocytosis. (A) Experimental outline depicting macrophage isolation from PBMCs, cytokine activation, and indirect co-culture with cancer or stromal cell secretome. (B) RFI (relative to Mϕ alone) of Siglec-10 expression on naïve, IFN-γ+IL-4, and IL-4 alone activated macrophages after indirect co-culture with HCT116 TCS or iTCS (n=4) with representative overlay histograms. The fluorescence minus one (FMO) control is represented by a black line histogram. (C) RFI (relative to Mϕ alone) of Siglec-10 expression in naïve, IFN-γ+IL-4, and IL-4 alone activated macrophages after indirect co-culture with $MSC^{TCS/iTCS}$ secretome (n=3) with representative overlay histogram. The FMO control is represented by a black line histogram. (D) Experimental outline of NAF and CAF direct co-culture with human PBMCs and sialic acid targeting with 3FAX or E610. (E) MFI of Siglec-10 expression by $CD11b^+$ macrophages after co-culture with NAFs and CAFs with or without E610 and 3FAX treatment (n=4). (F) % of red tumor cell uptake by macrophages was measured by live cell imaging over time and plotted as % of total cells. Representative graph showing % phagocytosis analyzed by Incucyte live cell imaging of pro-inflammatory macrophages or pro-inflammatory macrophages conditioned with TCS/iTCS (left) or MSC^{TCS}/MSC^{iTCS} secretome (right) over 24 hours. (G) Bar graph of the same experiment described in (F) showing quantification of phagocytosis at the 18 hour timepoint (n=2). Data are mean±SD; *p<0.05, **p<0.01, ***p<0.001, ****p<0.0001 using one-way ANOVA followed by Tukey's post hoc test. ANOVA, analysis of variance; CAF, cancer-associated fibroblast; FMO, fluorescence minus one; MFI, median fluorescence intensity; MSC, mesenchymal stromal cell; NAF, normal-associated fibroblast; PBMCs, peripheral blood mononuclear cells; RFI, relative fluorescence intensity; TCS, tumor cell secretome.

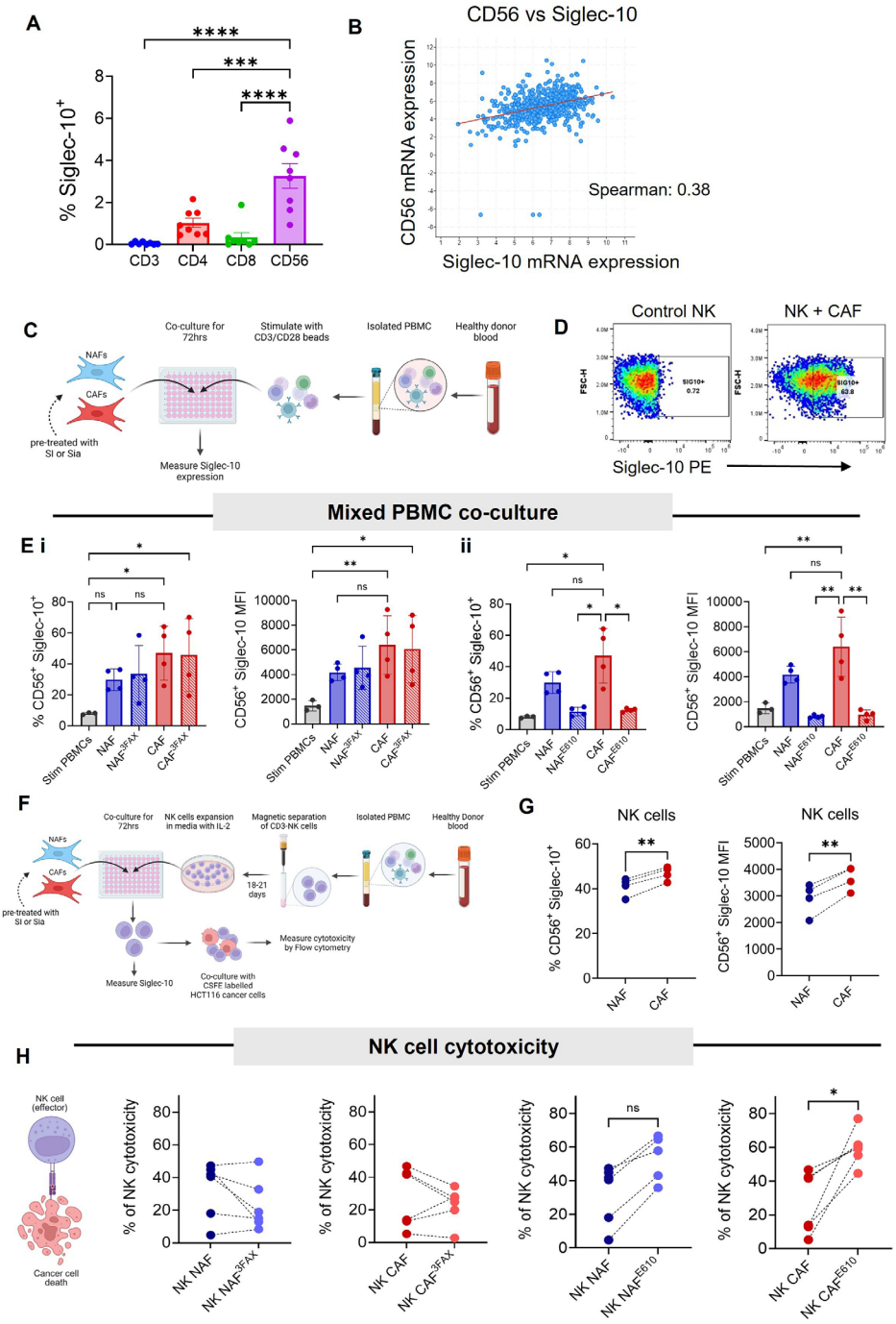

Figure 5 CAFs induce Siglec-10 on primary human NK cells, and targeting CAF sialylation increases NK cell anti-tumor function. (A) Frequency (%) of Siglec-10 expression by $CD3^+$ T cells, $CD4^+$ T cells, $CD8^+$ T cells, and $CD56^+$ NK cells (n=8). (B) Scatter plot showing the correlation between CD56 (NCAM1) and Siglec-10 mRNA expression in a cohort of 394 CRC patient samples from the TCGA database and analyzed using cBioPortal (https://www.cbioportal.org). (C) Experimental outline showing direct co-culture of NAFs or CAFs with stimulated human PBMCs. (D) Flow cytometry dot plots showing Siglec-10 expression by NK cells either cultured alone or following co-culture with CAFs. (E) (i) Frequency (%) (left) and MFI (right) of Siglec-10 expression by $CD56^+$ NK cells after co-culture with NAFs or CAFs with or without pre-treatment with 3FAX (n=4); (ii) Frequency (%) (left) and MFI (right) of Siglec-10 expression by $CD56^+$ NK cells after co-culture with NAFs or CAFs pretreated and cultured directly ± E610 (n=4). (F) Experimental outline showing NK cell isolation from PBMCs and direct co-culture with NAFs or CAFs, with or without 3FAX or E610 pre-treatment, followed by cytotoxicity assay setup. (G) Frequency (%) (left) and MFI (right) of Siglec-10 expression by $CD56^+$ NK cells after direct co-culture with NAFs or CAFs (n=4). (H) Percentage (%) of NK cytotoxicity, measured as the percentage of HCT116 cancer cell killing by NK cells post-co-culture with NAFs or CAFs, with or without 3FAX or E610 pre-treatment (n=5). Data are mean±SD; *p<0.05, **p<0.01, ***p<0.001; ****p<0.0001 by one-way ANOVA followed by Tukey's post hoc test (A, E) and paired t-test with Wilcoxon matched-pairs test (G, H). ANOVA, analysis of variance; CAF, cancer-associated fibroblast; MFI, median fluorescence intensity; NAF, normal-associated fibroblast; PBMCs, peripheral blood mononuclear cells.

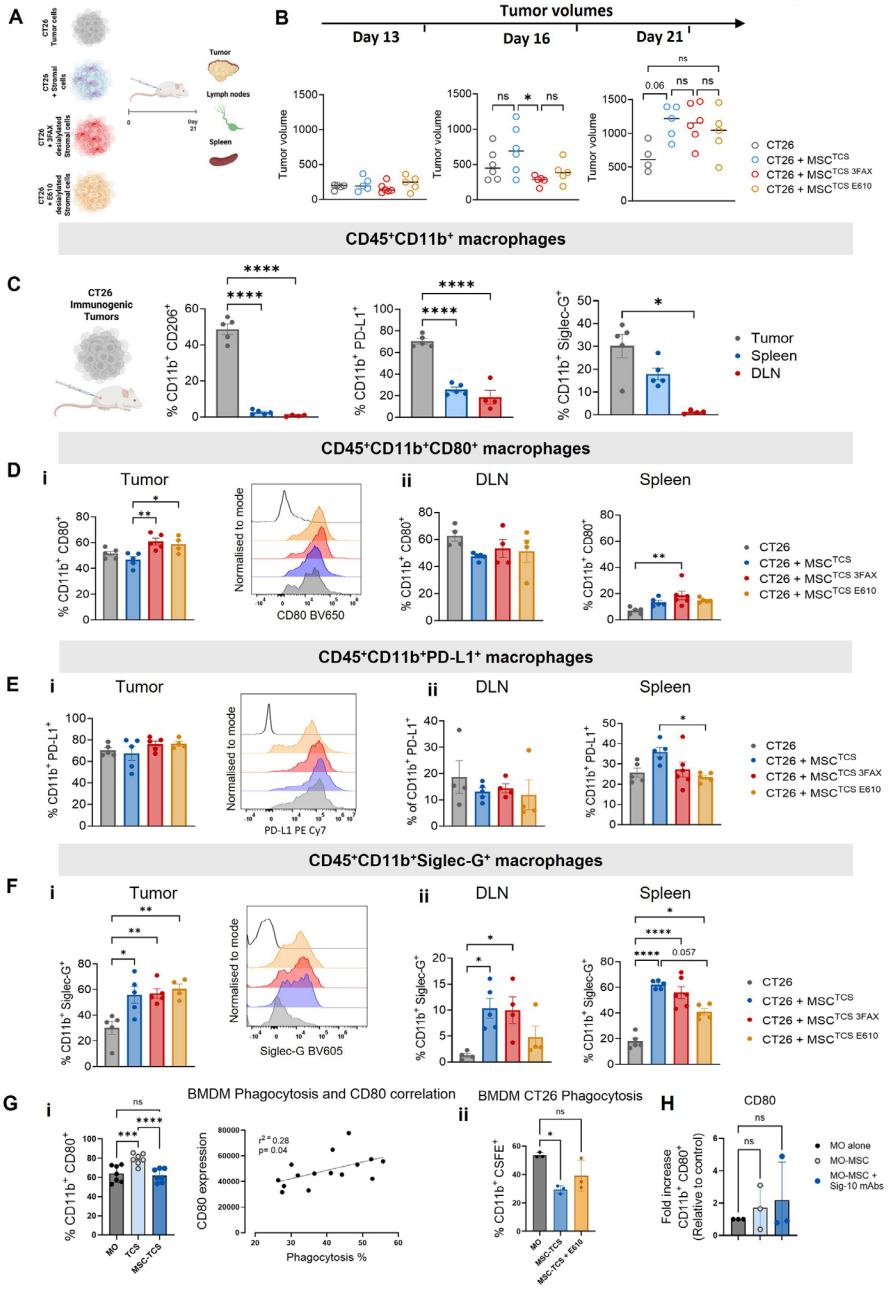

Figure 6 Targeting stromal cell sialylation increases Siglec-G expression by murine macrophages *in vivo*. (A) Experimental outline of murine tumor model. Balb/c mice were injected subcutaneously in the right flank with either CT26 cells alone, CT26+MSC^{TCS}, CT26+MSC$^{TCS\ 3FAX}$ or CT26+MSC$^{TCS\ E610}$. Tumors, spleens, and draining lymph nodes (DLNs) were harvested 21 days post-injection. (B) Tumor volume measured on day 13, day 16, and day 21. (C) Frequency (%) of CD206, PD-L1, and Siglec-G expression by CD45$^+$CD11b$^+$ macrophages in tumors, spleens, and DLNs of mice bearing CT26 tumors at day 21 post-injection. (D) (i) Frequency (%) of CD80 expression by CD45$^+$CD11b$^+$ macrophages in murine tumors at day 21 post-injection. Representative overlay histogram (right). (ii) Frequency (%) of CD80 expression by CD45$^+$CD11b$^+$ macrophages in DLNs and spleens of tumor-bearing mice at day 21 post-injection. (E) (i) Frequency (%) of PD-L1 expression by CD45$^+$CD11b$^+$ macrophages in murine tumors at day 21 post-injection. Representative overlay histogram shown on the right. (ii) Frequency (%) of PD-L1 expression by CD45$^+$CD11b$^+$ macrophages in DLNs and spleens of tumor-bearing mice (F) (i) Frequency (%) of Siglec-G expression by CD45$^+$CD11b$^+$ macrophages in murine tumors. Representative overlay histogram (right). (ii) Frequency (%) of Siglec-G expression by CD45$^+$CD11b$^+$ macrophages in DLNs and spleens of tumor-bearing mice. n=4–6 of biological replicates. (G) (i) Frequency (%) of CD11b$^+$CD80$^+$ cells in naïve murine bone marrow-derived macrophages (mBMDM) conditioned with TCS or MSC^{TCS} (left) and a scatter plot showing the correlation between CD80 expression and percentage phagocytosis (right). (ii) Percentage of CD11b$^+$CFSE$^+$ cells that represent phagocytosis events measured by flow cytometry of naïve macrophages conditioned with TCS ± E610 sialidase. (H) Frequency (%) of CD11b$^+$CD80$^+$ cells in human monocyte-derived macrophage:MSC co-culture ± Siglec-10 blocking. n=3–7. Data are mean±SD; *p<0.05, **p<0.01, ***p<0.001, ****p<0.0001 by one-way ANOVA followed by Tukey's post hoc test. ANOVA, analysis of variance; MSC, mesenchymal stromal cell; TCS, tumor cell secretome.

CD206$^+$, PD-L1,$^+$ and Siglec-G$^+$ macrophage phenotype. MSC^{TCS} did not significantly change the frequency of CD11b$^+$CD80$^+$ anti-tumor macrophages in the tumor; however, targeting sialylation increased the frequency of CD11b$^+$CD80$^+$ anti-tumor macrophages in both 3FAX and E610 pre-treated stromal cell groups (figure 6Di). This effect appeared to be tumor-specific, as it was not observed in the DLN (figure 6Dii), although an increase in CD11b$^+$CD80$^+$ macrophages was observed in the spleens of MSC^{TCS} 3FAX-pre-treated mice, although at much lower frequencies (figure 6Dii). The frequency of CD11b$^+$PD-L1$^+$ macrophages was higher in tumors compared with DLNs and spleens (figure 6Ei,ii); however, the frequency of CD11b$^+$PD-L1$^+$ macrophages was unchanged in the tumor and DLN, either by MSC^{TCS} or MSC^{TCS} 3FAX/E610 (figure 6Ei,ii). In the spleen, MSC^{TCS} induced higher frequencies of CD11b$^+$PD-L1$^+$ macrophages, which were reversed in MSC^{TCS} E610 pre-treated mice (figure 6Eii).

We next assessed the expression of the mouse ortholog of human Siglec-10, Siglec-G, on CD11b$^+$ macrophages. MSC^{TCS} tumors had significantly higher Siglec-G-expressing CD11b$^+$ macrophages, although this was not reversed by targeting stromal cell sialylation (figure 6Fi). We also observed significantly higher levels of Siglec-G-expressing CD11b$^+$ macrophages in the DLNs and spleens (figure 6Fii), which was reversed by targeting sialylation in the MSC^{TCS} E610 group specifically (figure 6Fii). These data suggest that targeting stromal sialylation alone is not sufficient to reduce Siglec-G expression on macrophages in the immunosuppressive TME, although Siglec G reduction is evident in the spleen. We then analyzed Siglec-G expression by pro-inflammatory and anti-inflammatory macrophage subsets, CD11b$^+$MHC-II$^+$CD206$^-$ and CD11b$^+$MHC-II$^+$CD206$^-$ in tumors (online supplemental figure 7Ai). Siglec-G expression was lower on pro-inflammatory macrophages than on anti-inflammatory macrophages (online supplemental figure 7Aii). Siglec-G expression was increased on both pro-inflammatory and anti-inflammatory macrophages in mice co-injected with MSC^{TCS}; however, no significant effect was observed by targeting stromal cell sialylation in the tumor (online supplemental figure 7Aii). Targeting stromal cell sialylation reversed the induction of Siglec-G on pro-inflammatory macrophages in the spleen, but not on anti-inflammatory macrophages (online supplemental figure 7Aiii). *Ex vivo*, to establish a direct link between targeting sialic acid on stromal cells and macrophage phagocytosis, we established a co-culture of mouse bone marrow-derived macrophages (BMDM) conditioned with tumor/stromal TCS. CT26 tumor cells were added, and phagocytosis and macrophage phenotype were assessed after 24 hours (online supplemental figure 7B). We observed that stromal cell conditioning suppressed CD80 expression on macrophages, which was associated with phagocytosis suppression. This suppression was reversed by targeting stromal cell sialylation with E610 sialidase. CD80 expression is positively correlated with enhanced phagocytosis in the *ex vivo* primary mouse assays (figure 6G). Additionally, in a human macrophage:MSC co-culture, we observed a trend increase in CD80 macrophage frequency following Siglec-10 blockade, indicating that Siglec-10 can modulate macrophage phenotype and potentially phagocytosis (figure 6H). Taken together, these data suggest that stromal cells induce an immunosuppressive macrophage phenotype in the CRC TME *in vivo*, characterized by CD206, PD-L1, and Siglec-G expression. Targeting stromal cell sialylation increased the frequency of activated CD80$^+$ macrophages in the tumor and a reduction of immunosuppressive phenotypes in the DLN and spleen, indicating a role in regulation of immunosuppression.

In vivo targeting of stromal cell sialylation increases cytotoxic NK cells

In CRC, NK cell infiltration has been identified as a positive prognostic marker in primary and metastatic disease.[53] Therefore, we assessed NK cell phenotype in tumor and secondary lymphoid tissues (DLN and spleen) to determine the effect of stromal cell sialylation on NK phenotype and function. NK cells were identified as CD45$^+$CD49b$^+$. Expression of the activation marker NKG2D, suppression marker Siglec-G, and cytolytic marker granzyme B was also assessed. We observed a higher overall frequency of CD49b$^+$ NK cells, as well as Siglec-G$^+$ and granzyme B$^+$-expressing CD49b$^+$ NK cells, in the tumor compared with secondary lymphoid tissues (figure 7A). Notably, NKG2D$^+$-activated NK cells were completely absent in the tumor, further supporting the highly immunosuppressive nature of the TME (figure 7A). We next evaluated the effect of stromal cell sialylation on NK cell infiltration. NK cell infiltration in MSC^{TCS} tumors was unaffected; however, targeting sialylation reversed this effect in MSC^{TCS} E610 pre-treated groups, significantly increasing NK cell infiltration (figure 7B), which was not observed in MSC^{TCS} 3FAX pretreated tumors (figure 7B). This finding indicates that sialylation of stromal cells plays a role in NK cell recruitment, which has been shown to have prognostic significance in CRC. Despite the increased NK cell infiltration, NKG2D$^+$ NK cells were absent in the tumor across all treatment groups, indicating that NK cells within the tumor remain inactivated (figure 7Ci). Interestingly, NKG2D$^+$ NK cells were present in the DLNs, with a trend toward higher levels observed in mice co-injected with MSC^{TCS} 3FAX and MSC^{TCS} E610 (figure 7Cii). This same trend was not observed in the spleen (data not shown). This suggests that stromal cell desialylation not only enhances NK cell recruitment but also promotes their local activation in secondary lymphoid tissues, which could be harnessed to optimize therapeutic approaches.

Siglec-G$^+$ NK cells were higher in CT26 tumors without stromal cells, reflecting the immunosuppressive TME associated with this model (figure 7D). Frequencies of Siglec-G$^+$ NK cells decreased in MSC^{TCS} and MSC^{TCS} 3FAX/E610 pre-treated tumors. The activity of NK cells in CRC, especially those expressing granzyme B, correlates

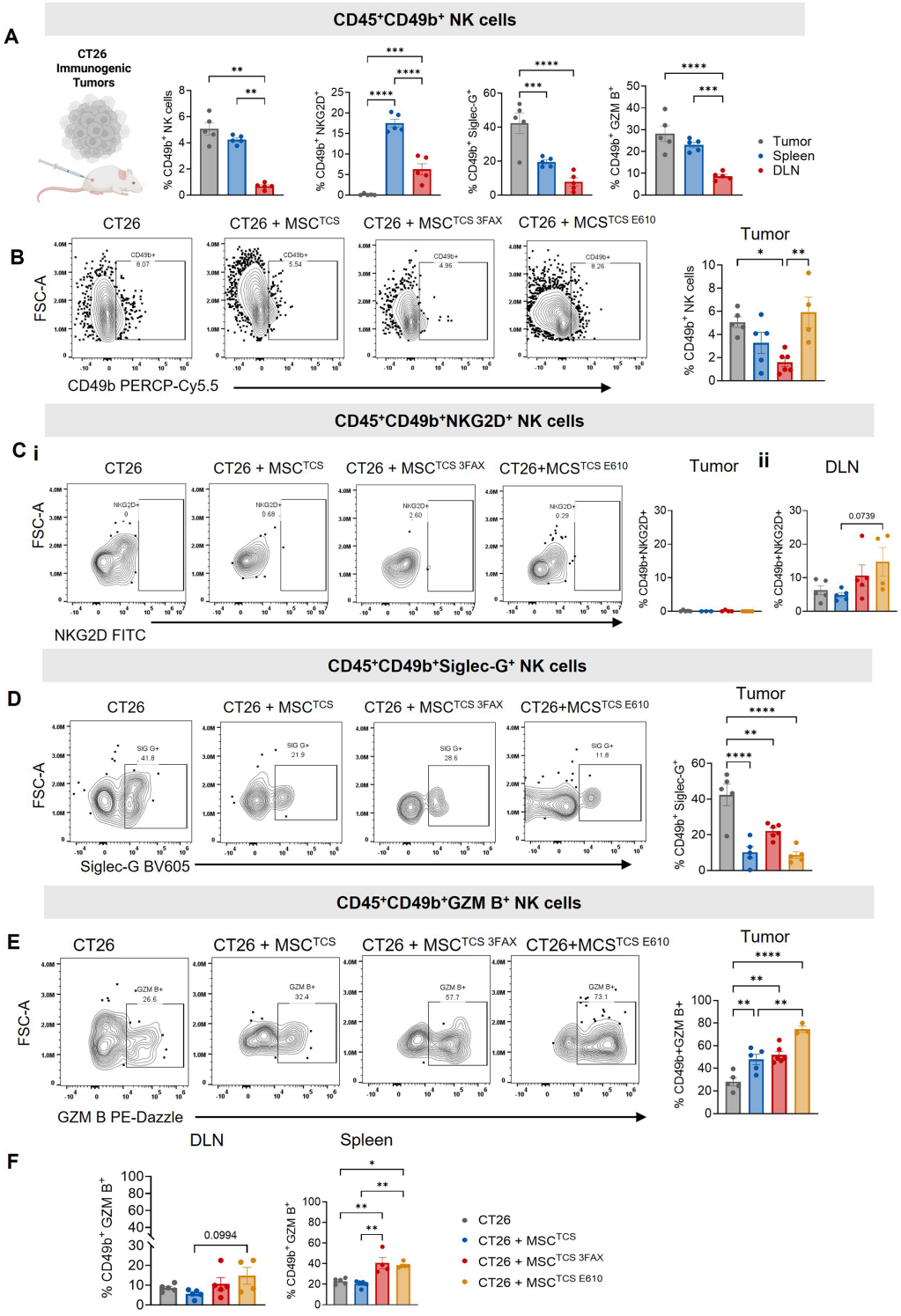

Figure 7 Targeting stromal cell sialylation *in vivo* increases NK cell granzyme B and reduces Siglec-G expression. (A) Frequency (%) of CD45$^+$CD49b$^+$ NK cells and NKG2D, Siglec-G, and granzyme B expression by CD45$^+$CD49b$^+$ NK cells in tumors, spleens, and DLNs of mice bearing CT26 tumors. (B) Representative flow cytometry contour plots and quantification of CD49b$^+$ NK cells in murine tumors following injection of CT26 cells alone, CT26 + MSC^{TCS}, CT26 + MSC$^{TCS\ 3FAX}$ or CT26 + MSC$^{TCS\ E610}$ at day 21 post-injection. (C) (i) Representative flow cytometry contour plots and quantification of NKG2D expression by CD49b$^+$ NK cells in murine tumors and (ii) DLNs. (D) Representative flow cytometry contour plots and quantification of Siglec-G expression by CD49b$^+$ NK cells in murine tumors. (E) Representative flow cytometry contour plots (left) and quantification of granzyme B expression by CD49b$^+$ NK cells in murine tumors (right). (F) Frequency (%) of Granzyme B (GZM-B) expression by CD49b$^+$ NK cells in DLNs and spleens of tumor-bearing mice at day 21 post-injection. Data are mean±SD; *p<0.05, **p<0.01, ***p<0.001, ****p<0.0001 by one-way ANOVA followed by Tukey's post hoc test. n=4–6 of biological replicates. ANOVA, analysis of variance; DLN, draining lymph nodes; MSC, mesenchymal stromal cell; TCS, tumor cell secretome.

with improved survival outcomes.[54] We observed that the frequencies of granzyme B$^+$ NK cells were increased in tumors from mice co-injected with MSC^{TCS} and further significantly increased in tumors from mice treated with MSC$^{TCS\ E610}$ but, interestingly, not MSC$^{TCS\ 3FAX}$ (figure 7E). Similar effects were seen systemically, where targeting stromal cell sialylation led to overall higher frequencies of granzyme B$^+$ NK cells in the spleens (figure 7F), thereby indicating restored cytolytic activity. This was not observed in the DLN, although trend increases are evident in tumors from MSC$^{TCS\ E610}$-pre-treated tumors (figure 7F). Our data suggest that stromal cell desialylation may enhance NK cell infiltration and may reprogram them toward an anti-tumor granzyme B-expressing expressing phenotype both locally in the tumor and secondary lymphoid tissues.

Inflammation alters the immune microenvironment in CRC and induces Siglec-G on macrophages and NK cells, which can be reversed by targeting the sialic acid/Siglec axis

Inflammation enhances stromal cell-mediated immunosuppression and is associated with CRC progression.[17 55] Analysis of the Biological Hallmark gene sets using GSEA on isolated epithelial and fibroblasts revealed that fibroblasts were significantly and specifically enriched in inflammatory response and TNF-α via NF-κB signaling (GSE39396, ConfoundR) (figure 8A). Furthermore, TNF-α signaling is enhanced in CMS4 CRC (Subtype ExploreR, FOCUS cohort) (figure 8B).[17] Therefore, to assess the impact of stromal-mediated inflammation on immune cell infiltration and activation, we co-injected CT26 cancer cells with MSC^{iTCS} or MSC^{iTCS} that were pre-treated with 3FAX prior to co-injection (figure 8C). Tumor cell invasion and NK and macrophage infiltration were assessed at day 13 in tumor, DLN, and spleen. We observed a significant increase in the frequency of Siglec-G-expressing macrophages and NK cells in MSC^{iTCS} tumors (figure 8D), which was dependent on stromal cell sialic acid, as it was completely reversed in 3FAX pre-treated stromal cell tumors. Strikingly similar trends were observed in both the DLNs (figure 8E) and spleens (figure 8F) of MSC^{iTCS} and MSC$^{iTCS\ 3FAX}$-treated mice. The level of expression of Siglec-G on both CD49b$^+$ and CD11b$^+$ cells was significantly higher in the tumor than the DLNs or spleens, indicating a predominant TME effect of immune cell Siglec receptor induction (data not shown). We next assessed Siglec-G expression on CD206$^+$ anti-inflammatory (figure 8G, left) and MHC-II$^+$ pro-inflammatory macrophages (figure 8G, right) and observed an induction of Siglec-G on both subsets of macrophages, which was reversed with 3FAX pre-treatment of stromal cells (figure 8G). Interestingly, 50% of mice co-injected with MSC^{iTCS} showed peritoneal invasion compared with no invasion in mice injected with CT26 cells alone (figure 8H). This was completely abrogated in mice co-injected with MSC$^{iTCS\ 3FAX}$ (figure 8H). These data show that targeting inflammatory tumor-conditioned stromal cell sialylation inhibits stromal cell-induced metastasis and reduces Siglec-G expression on macrophages and NK cells *in vivo*. We also show that targeting the sialic acid/Siglec axis locally can impact macrophage and NK cell phenotypes outside of the TME.

DISCUSSION

Sialoglycan-Siglec receptor interactions in the TME play an important role in driving immunosuppression and therapeutic resistance.[40] While aberrant sialylation of cancer cells has been well characterized,[39 56] the sialylation status and function of the tumor-supporting stroma is only beginning to be elucidated in different types of cancer/cancer models. We and others have shown previously that CRC and pancreatic ductal adenocarcinoma-derived CAFs express higher levels of sialoglycans when compared with tumor cells and cancer-adjacent NAFs, and these CAF sialoglycans are key modulators of CD8+T cells and myeloid cells, respectively.[20 24]

Using a combination of co-culture immunoassays, transcriptomic data from CRC patient datasets and an immunocompetent murine model of CRC, we investigated stromal cell sialylation in the context of CMS4 stromal-rich CRC. We assessed the functional impact on stromal cell-mediated modulation of innate immune cells, with a specific focus on macrophages and NK cells. GSEA analysis revealed that gene expression/signatures related to sialic acid binding, protein sialylation, and α2,3 ST activity were elevated on CMS4-like CRC patient tumors compared with CMS1-3. But, crucially, this same trend was not observed for global glycosylation-related gene sets. Given that CMS4-like CRC responds suboptimally to current therapies and has the worst overall prognosis compared with the other CMS subtypes,[5] this information provides insight that hypersialylation may play a key role in response to therapy. In fact, it has been demonstrated previously that sialylation of cell surface glycoproteins can significantly affect the ability of chemotherapy and radiotherapy to eliminate CC cells.[57] While multiple a2,3 and a2,6-specific STs are more highly expressed in stroma compared with epithelium in CRC patient samples, *ST6GALNAC6* was the most highly expressed. Furthermore, high expression of *ST6GALNAC6* correlates with significantly poorer survival in both non-classified CRC and CMS4-like CRC. The role of *ST6GALNAC6* in cancer appears to be dichotomous, with some studies reporting decreased expression of this ST in CRC[58] and malignant kidney cells[59] compared with normal epithelium, while others show decreased migratory capacity, as an indicator of metastatic ability, of renal carcinoma cells when *ST6GALNAC6* expression is silenced.[60] However, these studies did not assess *ST6GALNAC6* expression in the context of the stroma or stromal-rich tumors. We next sought to determine what effect *ST6GALNAC6* KD may have on expression of specific Siglec ligands. Interestingly, we found that shRNA-mediated KD of *ST6GALNAC6* significantly decreased expression of Siglec-10 ligands specifically. Therefore, we investigated

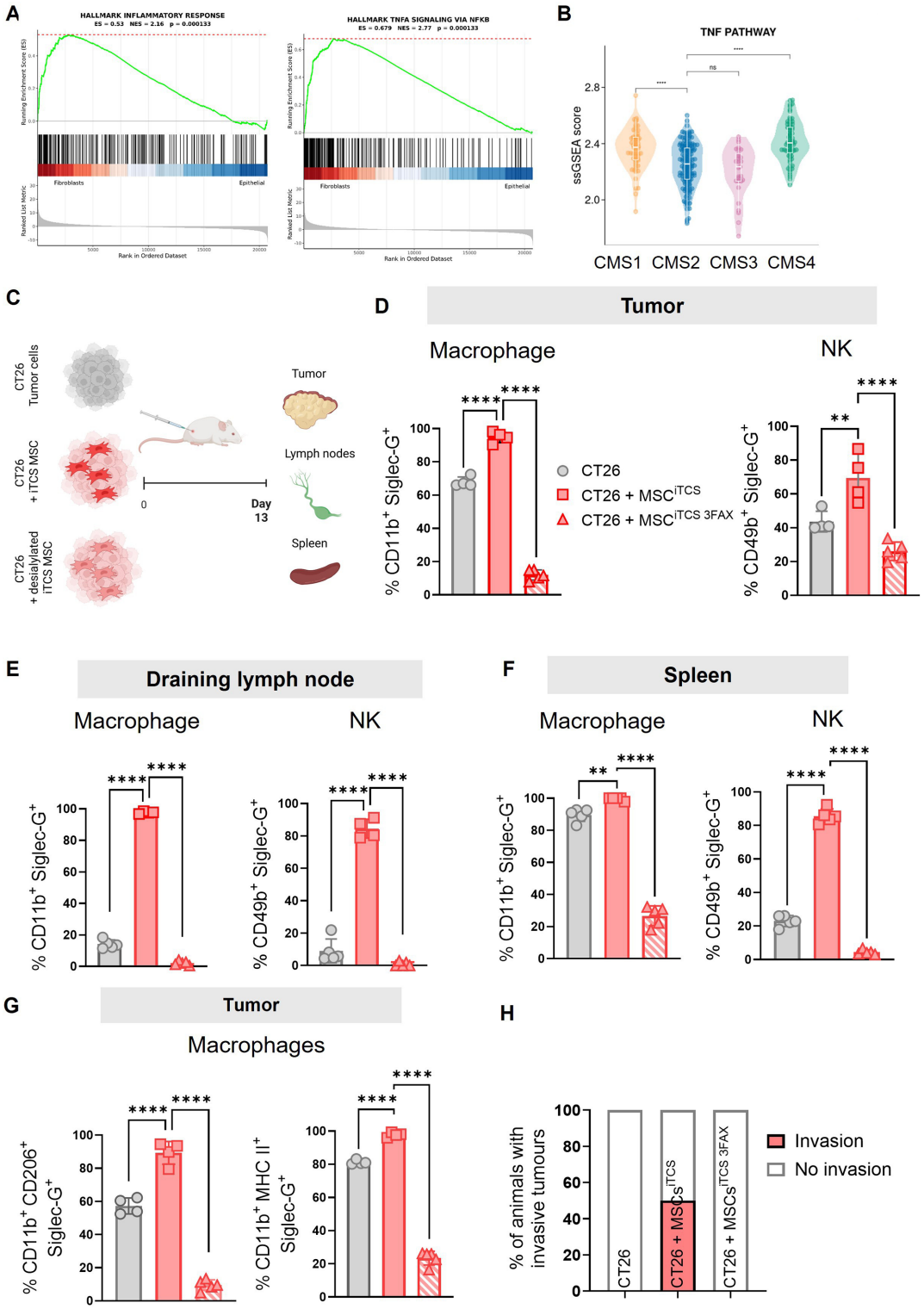

Figure 8 Targeting sialylation of stroma in inflammatory *in vivo* models of CRC reduces Siglec-G expression in tumor-infiltrating macrophages and NK cells. (A) GSEA data depicting hallmark inflammatory responses and hallmark TNF-α signaling via NK-κB in CRC tumors comparing transcriptional signatures in fibroblasts versus epithelial cells. (B) Transcriptional signatures of the TNF-α signaling pathway across CMS subtypes 1–4. (C) Experimental outline of murine tumor model. Balb/c mice were injected subcutaneously in the right flank with either CT26 cells alone or co-injected with MSC^{iTCS} or 3FAX pre-treated MSC ($MSC^{iTCS\ 3FAX}$). Tumors, spleens, and DLNs were harvested 13 days post-injection. Frequency (%) of Siglec-G expression by $CD11b^+$ macrophages or $CD49b^+$ NK cells in (D) tumors, (E) DLNs, and (F) spleens of tumor-bearing mice. (G) Frequency (%) of Siglec-G expression by $CD11b^+CD206^+$ pro- and $CD11b^+MHC\text{-}II^+$ anti-inflammatory macrophages in tumors. (H) Percentage (%) of mice with invasive tumors at Day 13. Data are mean±SD; **p<0.01, ****p<0.0001 using one-way ANOVA followed by Tukey's post hoc test. n=4–5 of biological replicates. ANOVA, analysis of variance; CMS, consensus molecular subtype; CRC, colorectal cancer; DLNs, draining lymph nodes; GSEA, gene set enrichment analysis; MSC, mesenchymal stromal cell.

Siglec-10 receptor expression in the context of stromal-dense CRC. In fibroblast-containing CRC tumors, we show that those with HiFi content are significantly higher expressers of Siglec-10 receptor compared with those with a low fibroblastic content. CRC patient tumors with HiFi content, coupled with high Siglec-10 expression, have poorer OS compared with LoFi CRC tumors with low Siglec-10 expression. Inflammatory tumor-conditioned MSCs (MSC^{iTCS}) show higher expression of Siglec-10 ligand compared with the cancer cells, demonstrating that Siglec-10 ligand expression is inducible. In addition, the known Siglec-10 ligands, CD24 and CD52, are also induced and expressed significantly higher on MSC^{iTCS}. This prompted us to perform a Siglec-10 receptor screen of different immune cell populations isolated from CRC patient-derived PBMCs. The data revealed that Siglec-10 was significantly more highly expressed on monocytes, macrophages, and NK cells.

There is a strong positive correlation between CD14 and Siglec-10 expression, demonstrated by analysis of CRC patient-derived PBMCs and by cBioPortal analysis of CRC patient cohorts. Siglec-10 receptor expression was induced on macrophages cultured in the presence of MSC^{iTCS}. The same induction was not observed when macrophages were cultured with HCT116 iTCS alone, indicating that paracrine factors secreted specifically from stromal cells exposed to the inflammatory tumor secretome were responsible for this effect. Two independent strategies were used to target sialylation on fibroblasts to assess what effects desialylation would have on Siglec-10 receptor expression on macrophages. While 3FAX pre-treatment of NAFs and CAFs had no observable effect on macrophage Siglec-10 expression following co-culture, sialic acid cleavage via E610 treatment led to a significant reduction in macrophage Siglec-10 expression. A potential explanation for these contrasting effects may be that 3FAX treatment prevented the trafficking of newly synthesized sialic acid to the fibroblast cell surface but had no effect on sialic acids already present on the cell surface, while sialidase treatment cleaved sialic acids directly, thereby resulting in reduced Siglec-10 ligand expression on NAFs and CAFs. In contrast to 3FAX, E610 acts on existing sialylated glycans and can rapidly expose epitopes and disrupt or reorganize receptor clustering after exposure, which may explain the differential effects of the two sialic acid-targeting approaches. Further research is required, however, to fully elucidate the mechanism of sialic acid generation in stromal cells. It may also indicate that exposure of immune cells to sialidase is also required for optimal effects.

$CD56^+$ NK cells express high levels of Siglec 10. Similar to our findings on macrophage Siglec-10 expression following co-culture with NAFs and CAFs treated with either 3FAX or E610, we observed the same effects on NK Siglec-10 expression. An additional noteworthy observation was that CAFs induced significantly higher frequencies of Siglec-10-expressing NK cells than NAFs following co-culture. Functionally direct cleavage of surface sialic acids on NAFs and CAFs by E610 yielded the most striking findings with regard to NK cell-mediated cytotoxicity of CRC cells. NK cells co-cultured with E610-treated CAFs were significantly more cytotoxic to CRC cells. This effect was not seen when NAFs and CAFs were treated with 3FAX prior to co-culture with NK cells. These data suggest that it may be worthwhile to target *ST6GALNAC6* specifically on CAFs (e.g., using CRISPR/Cas9-mediated gene knockout) and assess the effects on NK cells, as Kawasaki and colleagues have shown that *ST6GALNAC6*-knockout renal cell carcinoma cells are more susceptible to sialidase-treated NK cell lysis.[61] This may render CAFs more susceptible to killing by NK cells, which may subsequently create a path through the stromal-dense barrier for other relevant immune cell populations to target the cancer cells and exert their anti-tumor effects.

Using a subcutaneous mouse model of CRC to investigate the effects of co-administration of CRC cells with TCS-conditioned stromal cells with or without pre-treatment with 3FAX or E610, we observed lower tumor volumes in mice co-injected with desialylated stromal cells, regardless of the desialylating strategy used (i.e., 3FAX or E610), but with a more pronounced effect observed when stromal cells were treated with 3FAX prior to injection. These results show that removal of sialic acids, and potentially specific Siglec ligands, from the stroma leads to slower tumor growth over time. Similar findings, reported by Scott *et al*, demonstrated that *ST6GAL1* KD in prostate cancer cells led to suppression of tumor growth, and by Stanczak *et al* who showed inhibition of tumor progression in multiple mouse models by targeting tumor cell sialylation through the use of antibody-sialidase conjugates.[62 63] Assessing novel approaches to targeting sialic acid repeatedly may be more efficacious and give an insight into the kinetics of anti-tumor effects. We profiled specific immune cell subsets within the tumors, as well as key secondary lymphoid tissues (e.g., the draining inguinal lymph nodes and spleens). We observed increased CD80 expression on $CD11b^+$ macrophages in the tumor following stromal cell desialylation. Interestingly, in *ex vivo* cultures, we showed a direct correlation between CD80 expression and enhanced phagocytosis. We validated this finding in human macrophage:MSC co-cultures and additionally identified a role for Siglec-10 in the suppression of macrophage CD80. These observations indicate that targeting stromal cell sialylation can affect co-stimulatory molecule expression on macrophages and may subsequently enhance T-cell activation. These findings suggest that targeting sialylation may bridge both the innate and adaptive arms of the anti-tumor immune response to drive $CD8^+$ T cell responses.[20 64] In fact, Siglec 7 ligands have recently been identified as 'don't eat me signals'.[64]

Siglec-G, the murine orthologue of human Siglec-10,[26] is an inhibitory receptor involved in suppressing anti-tumor immune responses. *Ex vivo* analysis of Siglec-G expression by $CD11b^+$ macrophages within these tissues revealed that Siglec-G was significantly more highly induced in stromal-rich tumors as compared with CT26

tumors alone. A similar effect was seen in both the DLNs and spleen. Interestingly, E610-mediated desialylation of MSC^{TCS} prior to injection resulted in a clear reversal of this induction in secondary lymphoid tissues only. This shows for the first time, to the best of our knowledge, a sialic acid-mediated stromal cell-dependent induction of inhibitory Siglec-G on macrophages in an *in vivo* model of CRC. One possible explanation for why a similar reversal of Siglec-G expression on macrophages was not observed in the stromal-rich tumors in $MSC^{TCS\ E610}$ pre-treated mice could be due to the timepoint of this analysis (i.e., day 21 post-injection). Analysis of Siglec-G expression earlier in tumor development could provide further insight into the kinetics of expression and will be investigated in future studies. Our *in vivo* data also provided mechanistic insights into the role of sialylation in modulation of NK cell phenotype in stromal-rich CRC tumors. The most striking finding was the almost three-fold increase in granzyme B-expressing $CD49b^{+}$ NK cells in $MSC^{TCS\ E610}$ pre-treated tumors. A similar trend was seen in the spleens of tumor-bearing mice. Currently, there is limited information directly linking stromal cell sialylation to the modulation of granzyme B expression by NK cells. Further research is required to understand whether sialylation directly affects NK granzyme B expression or if it influences NK cell activity through interactions with target cells. Additionally, RNA expression data and PNA staining post-sialidase treatment indicate a role for *ST3GAL1*, which has been implicated in generation of Siglec-7 ligands, which are known to inhibit NK cells.[38] Incidentally, coexpression of *ST3GAL1* and *ST6GALNAC4* strongly indicates likely expression of Siglec-7 ligands, and further research is required to understand the specific role of *ST3Gal1* in tumor-associated stromal cells.

Finally, the impact of inflammatory conditioning of stromal cells was striking in the promotion of metastatic invasion in CT26 co-injected tumors, which was prevented by targeting stromal cell sialylation by 3FAX. These findings highlight that stromal cell sialylation, in addition to shaping anti-tumor immune phenotypes, may have a role in metastatic invasion of tumor cells. Further research is needed to understand the specific mechanisms involved. Taken together, these findings demonstrate that stromal cells have a strong capacity for innate immune cell modulation in CRC, which is regulated, at least in part, by sialylation. We have shown stromal cell-specific induction of Siglec-10 on both macrophages and NK cells, and targeting stromal cell sialylation with sialidase reversed this effect with a concomitant increase in anti-tumor effector function. Targeting stromal cell sialylation in CRC not only enhances anti-tumor immunity but also leads to slower tumor growth and inhibits metastasis *in vivo*. Targeting stromal cell sialylation in stromal-rich CMS4-like CRC may be key to reversing immunosuppression and enhancing response to anti-cancer therapies. Approaches such as anti-Siglec antibodies, sialidase-conjugated targeting antibodies (e.g., trastuzumab), antibody-conjugated nanoparticles, antibody-lectin chimeras to target the sialic acid/Siglec axis have shown promising anti-tumor efficacy in multiple cancer models.[65] These strategies could be further refined to target stromal cells, or even specific subsets of cancer-associated stromal cells (iCAF, myCAF, apCAF, etc), in combination with immunotherapeutics to overcome stromal-mediated immunosuppression.[65]

Limitations of this study

One limitation of this study is the lack of specificity when targeting stromal cell sialyation, as the two methods used (3FAX and E610) inhibit and cleave sialic acids non-discriminately and transiently. Longer-term, vector-mediated knockout of specific STs such as *ST6GALNAC6* on stromal cells or the use of monoclonal antibodies targeting Siglec-G in vivo or Siglec-10 in tumor xenografts *in vivo* would strengthen these findings.

METHODS

Human samples

CRC-derived NAFs and CAFs were isolated from tumor resections at University Hospital Galway as described.[20] Human PBMCs were isolated from fresh blood samples at University Hospital Galway. PBMCs were isolated by Ficoll-Paque (Cytiva Lifesciences) density gradient centrifugation as previously described.[20] Buffy coats containing the PBMCs were collected, resuspended in DPBS (Thermo Fisher Scientific), and kept on ice for further use.

Cell lines

Human colorectal cell lines HCT116, HT29, Caco-2, and SW480 were purchased from the American Type Culture Collection (ATCC). HCT116 and HT29 cells were cultured in McCoy's 5A media (Sigma-Aldrich), SW480 in RPMI-1640 media (Thermo Fisher Scientific) and Caco-2 in DMEM media (Sigma-Aldrich). All media were supplemented with 10% heat-inactivated-fetal bovine serum (HI-FBS) (Sigma-Aldrich), 1% L-glutamine, and 1% penicillin/streptomycin (Pen/Strep) (both from Sigma). Caco-2 cells were grown in DMEM-low glucose (Sigma-Aldrich) with 20% HI-FBS, 1% L-Glutamine, 1% Pen/Strep and 1% non-essential amino acid (NEAA) (Thermo Fisher Scientific). hTERT stromal cell line was a gift from Dr Meadhbh Brennan. hTERT cells were cultured in DMEM-high glucose containing sodium bicarbonate, L-glutamine, and sodium pyruvate (Sigma-Aldrich), supplemented with 10% FBS and 1% Pen Strep (Sigma Aldrich). Human cell master stocks were authenticated by ATCC, confirmed mycoplasma negative, expanded, frozen, and used within 20 passages.

Subcutaneous tumor model

Balb/c mice (8–14 weeks old, female) were purchased from Charles River (UK). To compare the effects of stromal cell sialylation in tumors, $5x10^5$ CT26 tumour cells were inoculated subcutaneously (s.c.) in the flank of mice under 2-3% isoflurane ± $1.5x10^5$ MSC^{TCS} or MSC^{iTCS} with or without pre-treatment with sialyltransferase inhibitor

(3FAX) (Biotechne) or sialidase E610-1A (Palleon Pharmaceuticals) in a total volume of 100 µl. Tumor growth was monitored daily, and size was measured 3x per week using a digital callipers. Tumor volume was calculated according to the rational ellipse formula: $(M^{1/2} \times M^2 \times \varpi/6)$. Mice with CT26 ± MSC^{iTCS} tumors were euthanized at day 13, while mice with CT26 ± MSC^{TCS} tumors ± 3FAX/E610 pre-treatment were euthanized at 21. At endpoint, tumors, draining lymph nodes (DLN), non-draining lymph nodes (NDLN) and spleens were harvested and assessed. The primary outcome measurement was immune cell activation. Mice were euthanized at endpoint or if tumors showed signs of ulceration or if clinical endpoint was reached. In the case of ulcer formation, mice were excluded from study analysis. See online supplemental file 2 for additional information.

Human MSC isolation and TCS conditioning

Human bone marrow-derived MSC (hMSCs) were isolated from healthy donors following ethical approval and informed consent and expanded as previously described[50] and cultured in MEM-α media (Thermo Fisher Scientific) supplemented with 10% FBS, 1% Pen/Strep, and 1 ng/mL hFGF-2 (PeproTech). The protocol to generate tumor and inflammatory tumor cells secretome (TCS and iTCS, respectively) and stromal cells conditioning was performed as previously described.[20]

ST inhibitor or sialidase treatment

$hMSC^{TCS/iTCS}$ or NAFs/CAFs were treated with 200 µM of the ST inhibitor 3FAX (Bio-Techne) in two rounds of a 72-hour treatment regimen, as previously described[20]. E610-1A sialidase (E610) was provided by Palleon Pharmaceuticals. $hMSC^{TCS/iTCS}$ or NAF/CAF were treated with 100 µg/mL E610 or IgG1 isotype control 24 hours before harvesting for analysis or inclusion in co-culture assays.

Isolation and polarization of primary human macrophage

Primary human macrophages were isolated from healthy donor PBMCs as previously described.[17 20] A total of 8×10^6 PBMCs were plated in 6-well low-adherence plates (Corning) in macrophage complete media (RPMI-1640 supplemented with 1% AB human serum and 1% Pen/Strep). After 2 days, non-adherent cells were washed away, and macrophages were cultured for 7 days with fresh media changes every 2–3 days. For conditioning, 1.5×10^5 macrophages on day 7 were plated in 24-well low-adherence plates (Corning) and polarized for 24 hours. The media were then replaced with a 50:50 mix of fresh macrophage complete media and TCS or iTCS. Macrophages were conditioned with TCS/iTCS for 2×72-hour incubations.

Isolation and expansion of primary NK cells

Primary human NK cells were isolated from healthy donor PBMCs using a human NK isolation kit and MACS LS column (Miltenyi Biotech) according to the manufacturer's protocol. Sorted NK cells were expanded in human NK MACS medium containing 1% AB human serum (ThermoFisher), 1% Pen Strep, and 500 IU/mL human recombinant IL-2 (PeproTech) for 18–21 days, with media changed or split every 2–3 days.

Transcriptional analysis of CRC datasets

The subset of the stage II/III untreated CC dataset (GSE39582)[66] (n=258) was previously downloaded and normalized.[42] The samples were classified into the CMS using the CMSclassifier package (V.1.0.0) (random forest method).[3] ssGSEA scores were generated using the GSVA package (V.1.38.2).[67] The gene sets used were retrieved from the Molecular Signatures Database[68 69] (accessed November 2022) and imported into R (V.R 4.0.5). The scores were scaled using the scale() function (default settings) in R with the gene sets as columns. R V.4.3.3 was used for visualization. The two packages used to generate heatmaps were ComplexHeatmap (V.2.18)[70] and circlize (V.0.4.16).[71] The boxplots were created using ggplot2 (V.3.5.1),[72] ggbeeswarm (V.0.7.2),[73] and statistically annotated by ggpubr (0.6.0). Wilcoxon rank sum test was used with CMS4 as the reference group. The ConfoundR and Subtype ExploreR web apps were used to generate and download figures. Visualization for figure 3A–D was created using R V.4.2.2. The previously mentioned cohort, GSE39582,[66] was used. The waterfall plots were created using the ggplot2 (V.3.5.1). The boxplots were created using ggplot2 (V.3.5.1),[72] ggbeeswarm (V.0.7.2),[73] and statistically annotated by ggpubr (V.0.6.0).[74] The statistical test used was the Wilcoxon rank sum test with CMS4 as the reference group. Kaplan-Meier plots were created using survminer (V.0.4.9)[14], the cutpoint was obtained using the surv_cutpoint() function and plots were created using the ggsurvplot() function. An additional cohort of stage II primary tumors from CRC patients (n=215) (E-MTAB-863), previously downloaded and normalized,[42] was used to validate bioinformatics analysis in figure 3. These samples were classified into CMS using the CMScaller R package.[75]

Correlation analysis

Correlation analysis was performed using Siglec-7, Siglec-9, and Siglec-10 expression vs FAP and PDPN expression. A Pearson correlation test was performed using the stats R package[76] and the correlation coefficient (r) and corresponding p values were extracted. Scatter plots were created using ggplot2 (V.3.5.1).[77]

Survival analysis

Kaplan-Meier plots were created using survminer (V.0.4.9).[78] The cutpoint was obtained using the surv_cutpoint() function, and plots were created using the ggsurvplot() function. The Cox proportional hazards method was also performed to calculate the HR and CIs for statistical group comparisons.

Multivariate analysis

Multivariate analysis was performed using the survivalAnalysis R package (V.0.4.0)[79] to evaluate the association between RFS and selected covariates in the stage II/III

untreated CC cohort. The model included *ST6GALNAC6* high and low splits based on the cutpoint value, CMS, sex, and TNM stage. RFS time and event status were used as outcome variables, and hazard ratios with 95% CIs were visualized using forest plots.

Stromal-immune cell direct co-cultures

NAF/CAF and PBMC co-cultures were performed as previously described.[20] Briefly, human PBMCs were resuspended in RPMI-1640 media containing 10% HI-FBS, 1% sodium pyruvate, 1% NEAA, 1% L-glutamine, 1% Pen/Strep, and 0.1% β-mercaptoethanol (all Sigma-Aldrich). Cells (1×10^5 cells/100 µL) were seeded in 96-well round-bottom plates with or without Human T-Activator CD3/CD28 Dynabeads (Thermo Fisher Scientific). 3FAX/E610 pre-treated NAFs/CAFs were added to lymphocytes (1×10^4 cells/100 µL; 1:10 ratio) in complete NAF/CAF medium. E610 was also added to co-culture wells with sialidase pre-treated cells except for the NK cell cytotoxicity assays. After 96 hours, cells were incubated with antibodies and analyzed using a Cytek Northern Lights Flow Cytometer (Cytek Biosciences). For NK cell co-cultures, 100 µL of NK cell suspension was added to 96-well U-bottom plates, followed by 100 µL of NAF/CAF suspension (1:2.5 NAF/CAF:NK ratio). After 72 hours, NK cells were analyzed by flow cytometry or used for cytotoxicity assays.

Isolation and culture of mouse BMDMs

Mouse BMDMs were isolated and cultured as previously described.[17] Briefly, Balb/c mice were euthanized by CO2 inhalation. Femurs and tibias were removed, cleaned of connective tissue, and placed in sterile DPBS. The bones were flushed with a 30G needle, clumps were filtered through 70 µm mesh filters and centrifuged at 400×g for 5 min. Red blood cells were removed using ACK lysis buffer (Thermo Fisher Scientific). Bone marrow cells were cultured at a density of 4.5×10^6 per well of a low-adherent 6-well plate (Corning) in macrophage medium for 6 days, with media changing every 2 days. Macrophage media consisted of 65% complete medium and 35% L929 condition medium, as previously described.[17] Complete media is RMPI-1640 supplemented with 10% HI-FBS, 1% sodium pyruvate, 1% NEAA (0.1 mmol/L), 1% L-glutamine (2 mmol/L), 1% penicillin (100 U/mL)/streptomycin (100 µg/mL), and 0.01% β-mercaptoethanol (55 µmol/L) (all from Sigma-Aldrich). L-929 conditioned medium, containing macrophage-colony stimulating factor (M-CSF), was collected from a 3-day culture of L929 cells. BMDMs were harvested after 6 days using 0.25% trypsin-EDTA (Thermo Fisher Scientific).

Indirect co-culture of mouse BMDM macrophage and MSC secretome

Mouse BMDMs were plated at 5×10^4 cells/well in 96-well flat bottom plates in macrophage media. After 24 hours, the media was changed to 50% complete macrophage media and 50% secretome from MSC or MSC^{TCS} with or without 100 µg/mL E610 and cultured for a further 72 hours. BMDMs were trypsinized, collected, and counted for analysis by flow cytometry or for downstream use in phagocytosis assays with cancer cells.

Mouse macrophage phagocytosis assay

Macrophages were cultured and conditioned as described above. 72 hours post-addition of stromal cell secretome, 2.5×10^4 CT26 cancer cells were added to each well. Prior to addition to the well, CT26 cells were labeled with CellTrace CFSE (Thermo Fisher Scientific) and heated at 65°C for 10 mins. Phagocytosis was assessed after 24 hours by flow cytometry by measuring the % of CD11b+CFSE+ cells.

Human macrophage phagocytosis assay

Primary human macrophages were isolated from fresh whole blood from healthy donor PBMCs as described above. Macrophages were then plated in 24-well plates for polarization into pro-inflammatory and anti-inflammatory phenotypes. Macrophages were conditioned with HCT116 TCS/iTCS or MSC TCS/iTCS. Following conditioning for 72 hours, macrophages were replated at 150,000 cells per well and allowed to adhere for 24 hours before 50,000 HCT116 cancer cells were added. HCT116 cancer cells were stained with pHRodo dye (Sartorius, pHrodo Incucyte Phagocytosis Kit). Plates were then placed in the Incucyte and live cell-imaged for 24 hours. Analysis was conducted using the Incucyte analysis software and macrophage uptake of pHrodo dye was measured and plotted as % of total cells with high cell area and mean low red intensity (plotted as % phagocytosis). As macrophages had lower red intensity and higher cell area than HCT116 cells, this was the exclusion criteria for analysis using the Incucyte software. Data were plotted as % phagocytosis over a time course of 24 hours.

NK cytotoxicity assay

HCT116 cancer cells were stained with CellTrace CFSE (Thermo Scientific) in DPBS for 10 mins at 37°C, followed by two washes with serum-containing media, then resuspended in complete HCT116 media. NK cells were centrifuged and resuspended in fresh NK cell media supplemented with 500 IU/mL human recombinant IL-2 (PeproTech). Then, 100 µL of HCT116 cell suspension was added to U-bottom 96-well plates (Sarstedt) at a concentration of 50,000 cells/well, followed by 100 µL of NK cells at a concentration of 100,000 cells/well to achieve a 2:1 effector-to-target ratio in 200 µL. After 16 hours, cancer cell death was measured by flow cytometry using Sytox Blue staining in CFSE+ cells. Cancer cell death was determined based on $CFSE^+Sytox^+$ cells.

shRNA KD of *ST6GALNAC6* in hTERT-MSCs

ST6GALNAC6 gene KD was achieved via lentiviral vector delivery of short hairpin RNA (shRNA). DNA plasmids for lentiviral production of shRNA (GeneCopoeia) were provided as clones encoding shRNA-targeting (KD) and a NT control. The shRNA plasmids were

transformed in TOP10F' *Escherichia coli* cells (ThermoFisher Scientific), expanded in LB broth, and the plasmid DNA was isolated using a plasmid Maxiprep kit (Invitrogen). Lentiviral vectors were produced in LentiX293 cells transfected with lentiviral plasmid DNA including shRNA plasmid and three lentiviral packaging plasmids (psPAX2.2, pMD2.G, and pRSV-Rev (Addgene)). After 18–24 hours, the culture medium was replaced, and the conditioned medium containing the lentiviral vector was harvested 48 and 72 hours post-transfection. Lentiviral supernatant was filtered and used to transduce hTERT-immortalized BM-MSCs in T25 flasks. Cells were incubated at 37°C for 72 hours, and GFP expression was measured to assess transduction efficiency. Transduced cells were selected with 50 µg/mL hygromycin (Sigma-Aldrich) for 8 days, expanded, and tested for *ST6GALNAC6* KD by RT-PCR and flow cytometry.

Real-time PCR (RT-PCR) analysis of *ST6GALNAC6* expression

RNA was isolated from *ST6GALNAC6* KD and NT hTERT MSCs using the Invitrogen PureLink RNA Mini Kit (Life Technologies), as per the manufacturer's instructions. cDNA synthesis was performed using 1 µg of isolated RNA. RT-PCR was performed using TaqMan *ST6GALNAC6* PCR primers (Life Technologies) and was run on the StepOne Plus system (Thermo Fisher Scientific). GAPDH was used as an internal control and relative expression levels were calculated using the ΔCT method.

Flow cytometric analysis of tumor, LNs, and spleen immune populations

The protocol for flow cytometric analysis of single cell suspensions isolated from tumor, spleen, draining, and non-DLNs from tumor-bearing mice was described in detail in our previous paper.[20] The detailed protocol and antibody information are provided in the online supplemental methods.

Statistical analysis

All analyses were conducted using GraphPad Prism V.10 (La Jolla, California, USA). Experiments were performed in triplicate unless stated otherwise in figure legends. Data were assessed for normal distribution using the Shapiro-Wilk normality test. Datasets containing two groups were analyzed by unpaired t-test, Mann-Whitney test, or paired t-test with Wilcoxon matched-pairs test where appropriate. Datasets containing three or more groups were analyzed by ordinary one-way analysis of variance (ANOVA) followed by Tukey's multiple comparison test, Kruskal-Wallis test, followed by Dunn's multiple comparisons test or two-way ANOVA with Sidak's multiple comparisons test, where appropriate and indicated. P values of <0.05 were considered significant across all statistical tests.

Additional methods details are available in online supplemental methods. Online supplemental file 3 outlines key resources used in this study.

Author affiliations
[1]Discipline of Pharmacology and Therapeutics, School of Medicine, College of Medicine, Nursing and Health Sciences, University of Galway, Galway, Ireland
[2]Regenerative Medicine Institute (REMEDI), School of Medicine, College of Medicine Nursing and Health Sciences, University of Galway, Galway, Ireland
[3]Lambe Institute for Translational Research, School of Medicine, College of Medicine, Nursing and Health Sciences, University of Galway, Galway, Ireland
[4]Patrick G Johnston Centre for Cancer Research, Queen's University Belfast, Belfast, UK
[5]Centre for Human Genetics, University of Oxford, Oxford, UK
[6]CÚRAM Centre for Research in Medical Devices, School of Medicine, College of Medicine, Nursing and Health Sciences, University of Galway, Galway, Ireland
[7]Palleon Pharmaceuticals, Waltham, MA 02451, USA
[8]Division of Anatomical Pathology, Galway University Hospital, Galway, Ireland
[9]Department of Colorectal Surgery, Galway University Hospital, Galway, Ireland
[10]Discipline of Pathology, School of Medicine, College of Medicine, Nursing and Health Sciences, University of Galway, Galway, Ireland
[11]Cancer Research UK Scotland Institute, Glasgow, UK
[12]Discipline of Medicine, School of Medicine, College of Medicine, Nursing and Health Sciences, University of Galway, Galway, Ireland

Acknowledgements All flow cytometry experiments were performed in the University of Galway Flow Cytometry Core Facility, which is supported by funds from the University of Galway, Research Ireland, the Irish Government's Programme for Research in Third Level Institutions, Cycle 5 and the European Regional Development Fund. The authors acknowledge the facilities and scientific and technical assistance of the Anatomy Imaging and Microscopy Facility at the University of Galway. Technical and consultative support for flow cytometry experiments was provided in the Lambe Institute for Translational Research at the University of Galway by Coralie Mureau and Catherine Loughrey. Graphics and animations created with BioRender, Microsoft PowerPoint, and Servier Medical Art. Servier Medical Art by Servier is licensed under a Creative Commons Attribution 3.0 Unported License (https://creativecommons.org/licenses/by/3.0/). The authors wish to thank the Bio-Resources Unit (BRU) technical, veterinary, and administrative staff in the University of Galway for facilitating *in vivo* studies and for their ongoing assistance, advice, and support in animal procedures, husbandry, care, and welfare. The authors would like to thank Lei Lei and Dr Clodagh O'Neill for their help with the *in vivo* study sample preparation. Finally, we wish to acknowledge and thank the patients who, following informed consent, provided samples for this study, for which we are extremely grateful.

Contributors AO'N, NZ and HE performed the majority of experiments and associated data analysis and manuscript writing. CB, SMC and PDD performed analysis on human CRC datasets and contributed to the interpretation of data and manuscript writing. NAL performed the Siglec screening analysis on immune cells and the associated data analysis. CO'M and LH performed the shRNA knockdown experiments. AW and ER were involved in the collection of data and processing and analysis of PBMCs and tumor biopsies. LP, LC and JC provided Sia/Siglec targeting reagents and contributed to the interpretation of data. MS, AC, KC, SOH and AMH contributed to study design, planned and performed surgical resections and biopsies and pathological assessment of the samples. LJE, TR and MO'D contributed to initial concept and study design, data interpretation and manuscript review. OT and AER conceived the study and contributed to study design, experimental planning, data interpretation, manuscript writing and AER is the guarantor.

Funding This work was funded by the Research Ireland Starting Investigator Grant and Frontiers for the Future Programme Award to Professor Aideen Ryan (15/SIRG/3456 and 19/FFP/6446) and an HRB-HRCI Irish Cancer Society Award to Professor's MO'D and AER (HRCI-HRB-2024-018). ER is supported by Science Foundation Ireland and the Engineering and Physical Sciences Research Council Centre for Doctoral Training in Engineered Tissues for Discovery, Industry and Medicine (Grant numbers 18/EPSRC-CDT/3583 and EP/S02347X/1). AW is supported by a Research Scholarship from the Irish Cancer Society (CRS22WAL).

Competing interests LP, JW-YC and LC are employees and shareholders of Palleon Pharmaceuticals. MO'D is a founder of ONK Therapeutics and a member of its Board of Directors and is coinventor on two related patents

(US20210186999A1 and US2017032727899A1). TR and AER are coinventors on patent US20210186999A1.

Patient consent for publication Not applicable.

Ethics approval Colorectal cancer biopsies and patient-matched blood samples were retrieved from patients undergoing colonic resection at Galway University Hospital under an ethically approved protocol (Clinical Research Ethics Committee, Ref: C.A. 2074 and C.A 3087). All participants gave written informed consent before samples were taken. PBMCs were isolated from the peripheral blood of donors attending a hemochromatosis clinic. Samples were collected under research protocols approved by the Clinical Research Ethics Committee at University Hospital Galway (Ref C.A. 2534). hMSCs were isolated from bone marrow samples following ethical approval (C.A. 02/08 -C.A. 429). All participants gave written informed consent before samples were taken.The subcutaneous murine tumor study was conducted following ethical approval by the Animal Care Research Ethics Committee (ACREC) of University of Galway (ACREC-17-Dec-04) and under individual and project authorization licences from the Health Products Regulatory Authority (HPRA) of Ireland (AE19125/P077).

Provenance and peer review Not commissioned; externally peer reviewed.

Data availability statement Data are available on reasonable request. This paper does not report original code. Any additional information required to reanalyze the data reported in this paper is available from the lead contact on reasonable request. Analysis and Associated Plots_.R package V.0.4.0 2025 (Available from: https://CRAN.R-project.org/package=survivalAnalysis).

Supplemental material This content has been supplied by the author(s). It has not been vetted by BMJ Publishing Group Limited (BMJ) and may not have been peer-reviewed. Any opinions or recommendations discussed are solely those of the author(s) and are not endorsed by BMJ. BMJ disclaims all liability and responsibility arising from any reliance placed on the content. Where the content includes any translated material, BMJ does not warrant the accuracy and reliability of the translations (including but not limited to local regulations, clinical guidelines, terminology, drug names and drug dosages), and is not responsible for any error and/or omissions arising from translation and adaptation or otherwise.

ORCID iDs
Aoise O'Neill http://orcid.org/0009-0004-2390-1351
Norashikin Zakaria http://orcid.org/0000-0003-2589-1543
Clodagh O'Meara http://orcid.org/0009-0003-4123-2799
Linda Howard http://orcid.org/0000-0003-4760-7996
Jenny Che http://orcid.org/0009-0000-3181-0848
Lizhi Cao http://orcid.org/0000-0003-3725-0057
Thomas Ritter http://orcid.org/0000-0001-7709-8489
Oliver Treacy http://orcid.org/0000-0003-3898-9806
Aideen E Ryan http://orcid.org/0000-0002-5831-6783

REFERENCES

1 Siegel RL, Giaquinto AN, Jemal A. Cancer statistics, 2024. *CA Cancer J Clin* 2024;74:12–49.
2 Yan S, Wang W, Feng Z, *et al*. Immune checkpoint inhibitors in colorectal cancer: limitation and challenges. *Front Immunol* 2024;15:1403533.
3 Guinney J, Dienstmann R, Wang X, *et al*. The consensus molecular subtypes of colorectal cancer. *Nat Med* 2015;21:1350–6.
4 Ten Hoorn S, de Back TR, Sommeijer DW, *et al*. Clinical Value of Consensus Molecular Subtypes in Colorectal Cancer: A Systematic Review and Meta-Analysis. *J Natl Cancer Inst* 2022;114:503–16.
5 Peters NA, Constantinides A, Ubink I, *et al*. Consensus molecular subtype 4 (CMS4)-targeted therapy in primary colon cancer: A proof-of-concept study. *Front Oncol* 2022;12:969855.
6 Mouillet-Richard S, Cazelles A, Sroussi M, *et al*. Clinical Challenges of Consensus Molecular Subtype CMS4 Colon Cancer in the Era of Precision Medicine. *Clin Cancer Res* 2024;30:2351–8.
7 Mayer S, Milo T, Isaacson A, *et al*. The tumor microenvironment shows a hierarchy of cell-cell interactions dominated by fibroblasts. *Nat Commun* 2023;14:5810.
8 Jenkins L, Jungwirth U, Avgustinova A, *et al*. Cancer-Associated Fibroblasts Suppress CD8+ T-cell Infiltration and Confer Resistance to Immune-Checkpoint Blockade. *Cancer Res* 2022;82:2904–17.
9 Li T, Yi S, Liu W, *et al*. Colorectal carcinoma-derived fibroblasts modulate natural killer cell phenotype and antitumor cytotoxicity. *Med Oncol* 2013;30:663.
10 Kondo Y, Suzuki S, Takahara T, *et al*. Improving function of cytotoxic T-lymphocytes by transforming growth factor-β inhibitor in oral squamous cell carcinoma. *Cancer Sci* 2021;112:4037–49.
11 Takahashi H, Sakakura K, Kudo T, *et al*. Cancer-associated fibroblasts promote an immunosuppressive microenvironment through the induction and accumulation of protumoral macrophages. *Oncotarget* 2017;8:8633–47.
12 Chakravarthy A, Khan L, Bensler NP, *et al*. TGF-β-associated extracellular matrix genes link cancer-associated fibroblasts to immune evasion and immunotherapy failure. *Nat Commun* 2018;9:4692.
13 Costa A, Kieffer Y, Scholer-Dahirel A, *et al*. Fibroblast Heterogeneity and Immunosuppressive Environment in Human Breast Cancer. *Cancer Cell* 2018;33:463–79.
14 Zeng D, Wang M, Wu J, *et al*. Immunosuppressive Microenvironment Revealed by Immune Cell Landscape in Pre-metastatic Liver of Colorectal Cancer. *Front Oncol* 2021;11:620688.
15 Geyer M, Gaul L-M, D Agosto SL, *et al*. The tumor stroma influences immune cell distribution and recruitment in a PDAC-on-a-chip model. *Front Immunol* 2023;14:1155085.
16 Wu J, Liu X, Reeser JAW, *et al*. Stromal p53 Regulates Breast Cancer Development, the Immune Landscape, and Survival in an Oncogene-Specific Manner. *Mol Cancer Res* 2022;20:1233–46.
17 Leonard NA, Corry SM, Reidy E, *et al*. Tumor-associated mesenchymal stromal cells modulate macrophage phagocytosis in stromal-rich colorectal cancer via PD-1 signaling. *iScience* 2024;27:110701.
18 Turley SJ, Cremasco V, Astarita JL. Immunological hallmarks of stromal cells in the tumour microenvironment. *Nat Rev Immunol* 2015;15:669–82.
19 Mellman I, Chen DS, Powles T, *et al*. The cancer-immunity cycle: Indication, genotype, and immunotype. *Immunity* 2023;56:2188–205.
20 Egan H, Treacy O, Lynch K, *et al*. Targeting stromal cell sialylation reverses T cell-mediated immunosuppression in the tumor microenvironment. *Cell Rep* 2023;42:112475.
21 Ye J, Baer JM, Faget DV, *et al*. Senescent CAFs Mediate Immunosuppression and Drive Breast Cancer Progression. *Cancer Discov* 2024;14:1302–23.
22 Zhang L, Cascio S, Mellors JW, *et al*. Single-cell analysis reveals the stromal dynamics and tumor-specific characteristics in the microenvironment of ovarian cancer. *Commun Biol* 2024;7:20.
23 Agorku DJ, Bosio A, Alves F, *et al*. Colorectal cancer-associated fibroblasts inhibit effector T cells via NECTIN2 signaling. *Cancer Lett* 2024;595:216985.
24 Boelaars K, Rodriguez E, Huinen ZR, *et al*. Pancreatic cancer-associated fibroblasts modulate macrophage differentiation via sialic acid-Siglec interactions. *Commun Biol* 2024;7:430.
25 Rodriguez E, Boelaars K, Brown K, *et al*. Sialic acids in pancreatic cancer cells drive tumour-associated macrophage differentiation via the Siglec receptors Siglec-7 and Siglec-9. *Nat Commun* 2021;12:1270.
26 van de Wall S, Santegoets KCM, van Houtum EJH, *et al*. Sialoglycans and Siglecs Can Shape the Tumor Immune Microenvironment. *Trends Immunol* 2020;41:274–85.
27 Zhu W, Zhou Y, Guo L, *et al*. Biological function of sialic acid and sialylation in human health and disease. *Cell Death Discov* 2024;10:415.
28 Bärenwaldt A, Läubli H. The sialoglycan-Siglec glyco-immune checkpoint - a target for improving innate and adaptive anti-cancer immunity. *Expert Opin Ther Targets* 2019;23:839–53.
29 Crocker PR, Paulson JC, Varki A. Siglecs and their roles in the immune system. *Nat Rev Immunol* 2007;7:255–66.
30 Pillai S, Netravali IA, Cariappa A, *et al*. Siglecs and immune regulation. *Annu Rev Immunol* 2012;30:357–92.
31 Li X, Tian W, Jiang Z, *et al*. Targeting CD24/Siglec-10 signal pathway for cancer immunotherapy: recent advances and future directions. *Cancer Immunol Immunother* 2024;73:31.
32 Barkal AA, Brewer RE, Markovic M, *et al*. CD24 signalling through macrophage Siglec-10 is a target for cancer immunotherapy. *Nature New Biol* 2019;572:392–6.
33 Yin S, Li C, Shen X, *et al*. Siglec-G Suppresses CD8 $^{+}$ T Cells Responses through Metabolic Rewiring and Can be Targeted to Enhance Tumor Immunotherapy . *Adv Sci (Weinh)* 2024;11:e2403438.
34 Xiao R, Tian Y, Zhang J, *et al*. Increased Siglec-9/Siglec-9L interactions on NK cells predict poor HCC prognosis and

present a targetable checkpoint for immunotherapy. *J Hepatol* 2024;80:792–804.
35 Li S, Chen D, Guo H, *et al*. IMM47, a humanized monoclonal antibody that targets CD24, exhibits exceptional anti-tumor efficacy by blocking the CD24/Siglec-10 interaction and can be used as monotherapy or in combination with anti-PD1 antibodies for cancer immunotherapy. *Antibody Therapeutics* 2023;6:240–52.
36 Stanczak MA, Läubli H. Siglec receptors as new immune checkpoints in cancer. *Mol Aspects Med* 2023;90:101112.
37 O'Dwyer M, Kirkham-McCarthy L, Cerreto M, *et al*. PSGL-1 decorated with sialyl Lewis$^{a/x}$ promotes high affinity binding of myeloma cells to P-selectin but is dispensable for E-selectin engagement. *Sci Rep* 2024;14:1756.
38 Daly J, Sarkar S, Natoni A, *et al*. Targeting hypersialylation in multiple myeloma represents a novel approach to enhance NK cell-mediated tumor responses. *Blood Adv* 2022;6:3352–66.
39 Marciel MP, Haldar B, Hwang J, *et al*. Role of tumor cell sialylation in pancreatic cancer progression. *Adv Cancer Res* 2023;157:123–55.
40 Gonzalez-Gil A, Schnaar RL. Siglec Ligands. *Cells* 2021;10:1260.
41 Fessler E, Medema JP. Colorectal Cancer Subtypes: Developmental Origin and Microenvironmental Regulation. *Trends Cancer* 2016;2:505–18.
42 Corry SM, McCorry AM, Lannagan TR, *et al*. Activation of innate-adaptive immune machinery by poly(I:C) exposes a therapeutic vulnerability to prevent relapse in stroma-rich colon cancer. *Gut* 2022;71:2502–17.
43 Győrffy B. Integrated analysis of public datasets for the discovery and validation of survival-associated genes in solid tumors. *Innovation (Camb)* 2024;5:100625.
44 Boelaars K, van Kooyk Y. Targeting myeloid cells for cancer immunotherapy: Siglec-7/9/10/15 and their ligands. *Trends Cancer* 2024;10:230–41.
45 Läubli H, Kawanishi K, George Vazhappilly C, *et al*. Tools to study and target the Siglec-sialic acid axis in cancer. *FEBS J* 2021;288:6206–25.
46 Zu S, Lu Y, Xing R, *et al*. Changes in subset distribution and impaired function of circulating natural killer cells in patients with colorectal cancer. *Sci Rep* 2024;14:12188.
47 Zhang R, Qi F, Zhao F, *et al*. Cancer-associated fibroblasts enhance tumor-associated macrophages enrichment and suppress NK cells function in colorectal cancer. *Cell Death Dis* 2019;10:273.
48 Jandus C, Boligan KF, Chijioke O, *et al*. Interactions between Siglec-7/9 receptors and ligands influence NK cell-dependent tumor immunosurveillance. *J Clin Invest* 2014;124:1810–20.
49 Majid U, Bergsland CH, Sveen A, *et al*. The prognostic effect of tumor-associated macrophages in stage I-III colorectal cancer depends on T cell infiltration. *Cell Oncol* 2024;47:1267–76.
50 O'Malley G, Treacy O, Lynch K, *et al*. Stromal Cell PD-L1 Inhibits CD8$^+$ T-cell Antitumor Immune Responses and Promotes Colon Cancer. *Cancer Immunol Res* 2018;6:1426–41.
51 Kim H-D, Kim SY, Kim J, *et al*. Dynamic increase of M2 macrophages is associated with disease progression of colorectal cancers following cetuximab-based treatment. *Sci Rep* 2022;12:1678.
52 Yin Y, Liu B, Cao Y, *et al*. Colorectal Cancer-Derived Small Extracellular Vesicles Promote Tumor Immune Evasion by Upregulating PD-L1 Expression in Tumor-Associated Macrophages. *Adv Sci (Weinh)* 2022;9:2102620.
53 Donadon M, Hudspeth K, Cimino M, *et al*. Increased Infiltration of Natural Killer and T Cells in Colorectal Liver Metastases Improves Patient Overall Survival. *J Gastrointest Surg* 2017;21:1226–36.
54 Väyrynen JP, Haruki K, Lau MC, *et al*. Spatial Organization and Prognostic Significance of NK and NKT-like Cells via Multimarker Analysis of the Colorectal Cancer Microenvironment. *Cancer Immunol Res* 2022;10:215–27.
55 Burgos-Molina AM, Téllez Santana T, Redondo M, *et al*. The Crucial Role of Inflammation and the Immune System in Colorectal Cancer Carcinogenesis: A Comprehensive Perspective. *Int J Mol Sci* 2024;25:6188.
56 Büll C, den Brok MH, Adema GJ. Sweet escape: sialic acids in tumor immune evasion. *Biochim Biophys Acta* 2014;1846:238–46.
57 Park JJ, Lee M. Increasing the α 2, 6 Sialylation of Glycoproteins May Contribute to Metastatic Spread and Therapeutic Resistance in Colorectal Cancer. *Gut Liver* 2013;7:629–41.
58 Miyazaki K, Ohmori K, Izawa M, *et al*. Loss of disialyl Lewis(a), the ligand for lymphocyte inhibitory receptor sialic acid-binding immunoglobulin-like lectin-7 (Siglec-7) associated with increased sialyl Lewis(a) expression on human colon cancers. *Cancer Res* 2004;64:4498–505.
59 Senda M, Ito A, Tsuchida A, *et al*. Identification and expression of a sialyltransferase responsible for the synthesis of disialylgalactosylgloboside in normal and malignant kidney cells: downregulation of ST6GalNAc VI in renal cancers. *Biochem J* 2007;402:459–70.
60 Hugonnet M, Singh P, Haas Q, *et al*. The Distinct Roles of Sialyltransferases in Cancer Biology and Onco-Immunology. *Front Immunol* 2021;12:799861.
61 Kawasaki Y, Ito A, Kakoi N, *et al*. Ganglioside, disialosyl globopentaosylceramide (DSGb5), enhances the migration of renal cell carcinoma cells. *Tohoku J Exp Med* 2015;236:1–7.
62 Scott E, Archer Goode E, Garnham R, *et al*. ST6GAL1-mediated aberrant sialylation promotes prostate cancer progression. *J Pathol* 2023;261:71–84.
63 Stanczak MA, Rodrigues Mantuano N, Kirchhammer N, *et al*. Targeting cancer glycosylation repolarizes tumor-associated macrophages allowing effective immune checkpoint blockade. *Sci Transl Med* 2022;14:eabj1270.
64 Lenschow DJ, Walunas TL, Bluestone JA. CD28/B7 system of T cell costimulation. *Annu Rev Immunol* 1996;14:233–58.
65 O'Neill A, Zakaria N, Egan H, *et al*. The Tumour Glyco-Code: Sialylation as a Mediator of Stromal Cell Immunosuppression in the Tumour Microenvironment. *Eur J Immunol* 2025;55:e70000.
66 Marisa L, de Reyniès A, Duval A, *et al*. Gene expression classification of colon cancer into molecular subtypes: characterization, validation, and prognostic value. *PLoS Med* 2013;10:e1001453.
67 Hänzelmann S, Castelo R, Guinney J. GSVA: gene set variation analysis for microarray and RNA-seq data. *BMC Bioinformatics* 2013;14:7.
68 Liberzon A, Subramanian A, Pinchback R, *et al*. Molecular signatures database (MSigDB) 3.0. *Bioinformatics* 2011;27:1739–40.
69 Subramanian A, Tamayo P, Mootha VK, *et al*. Gene set enrichment analysis: a knowledge-based approach for interpreting genome-wide expression profiles. *Proc Natl Acad Sci U S A* 2005;102:15545–50.
70 Gu Z, Eils R, Schlesner M. Complex heatmaps reveal patterns and correlations in multidimensional genomic data. *Bioinformatics* 2016;32:2847–9.
71 Gu Z, Gu L, Eils R, *et al*. circlize Implements and enhances circular visualization in R. *Bioinformatics* 2014;30:2811–2.
72 Wickham H. ggplot2: elegant graphics for data analysis. New York: Springer-Verlag, 2016.
73 Clarke E. ggbeeswarm: categorical scatter (violin point) plots, version 0.7.2. 2023.
74 Kassambara A. ggpubr: "ggplot2" based publication ready plots. CRAN; 2023.
75 Eide PW, Bruun J, Lothe RA, *et al*. CMScaller: an R package for consensus molecular subtyping of colorectal cancer pre-clinical models. *Sci Rep* 2017;7:16618.
76 Team, R.C. R: a language and environment for statistical computing. R foundation for statistical computing, Vienna, Austria. 2022. Available: https://www.R-project.org/
77 Wickham, ggplot2: elegant graphics for data analysis: springer-verlag New York. 2016.
78 Kassambara A, Kosinski M. B. P. survminer: drawing survival curves using "ggplot2", R package version 0.5.0. 2024. Available: https://rpkgs.datanovia.com/survminer/index.html
79 Wiesweg M. survivalAnalysis: high-level interface for survival analysis and associated Plots_.R package version 0.4.0, 2025. Available: https://CRAN.R-project.org/package=survivalAnalysis